INTRODUCTION

Nowadays, small-scale decentralised distributed generation systems are on track to become the foundation of the worldwide energy network and it is a promising alternative solution to the typical large-scale centralised power plants. Consequently, microgrid systems comprising of a hybrid renewable energy system (HRES) can play a significant role in satisfying the energy demands of remote regions and resolving the energy price inflation and environmental problems posed by the use of fossil fuels in energy production (Motevasel et al., 2013). Therefore, microgrids with HRES would help to eliminate over a hundred million tonnes of CO_2 emissions from the atmosphere each year by providing a reliable, sustainable, and cost-competitive renewable energy supply, thus meeting the global energy needs without compromising the planet's well-being. For instance, integration of HRES with energy storage systems, such as batteries and traditional power systems, such as a boiler or diesel engine into microgrid is considered the popular way of increasing the reliability to meet the energy demand (Belfkira et al., 2011; Kumar et al., 2013), as depicted in Figure 1 (Kabalci, 2021). In consequence, the HRES microgrids are more reliable and economical when compared to the single renewable energy system (Dufo-López et al., 2011).

Figure 1. Microgrid with its multiple demand and source connections (Kabalci, 2021).

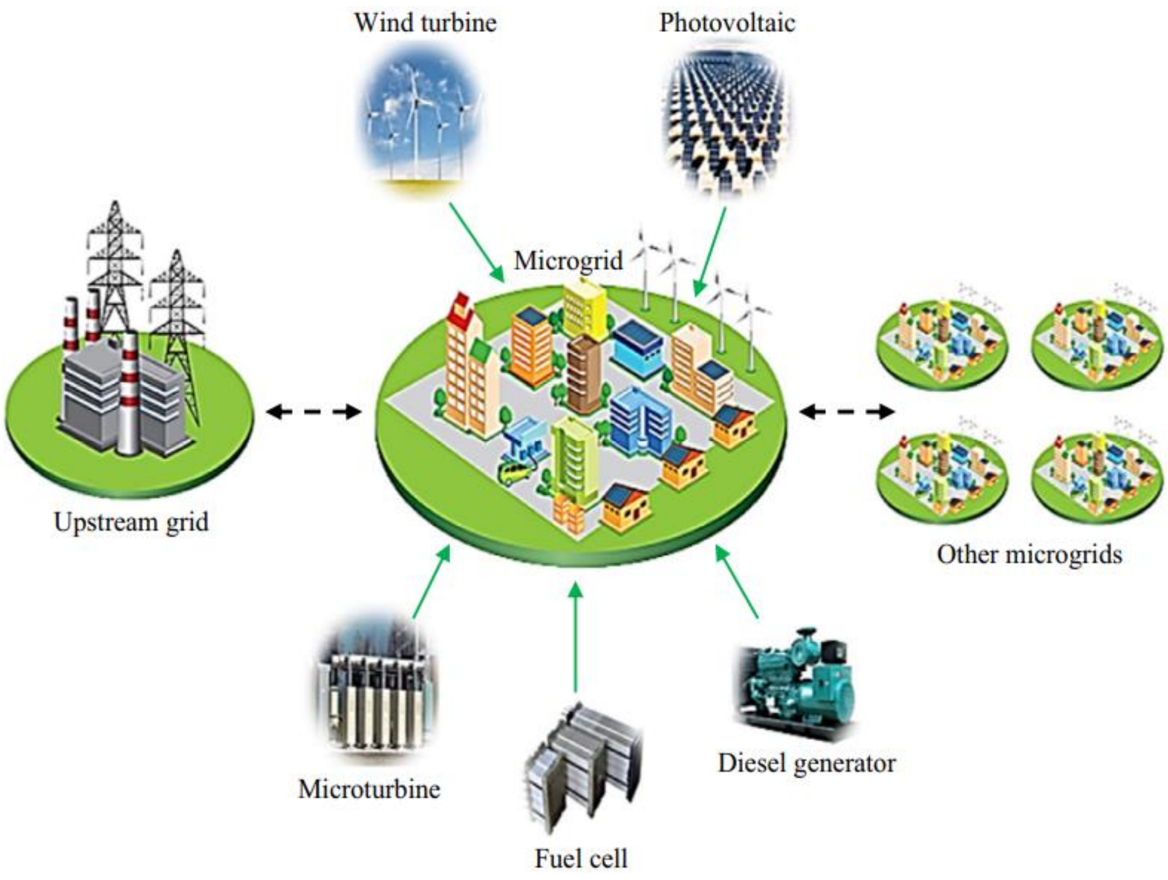

Solar and wind energy resources are widely used in microgrids. Nevertheless, these resources need proper management in order to facilitate their power operations to mitigate the implications of the intermittent output. To fully utilise this process, the sizing optimisation methodologies should be applied by a suitable selection of the governing parameters to obtain an optimal hybrid system design. Therefore, the optimised system will be economical, efficient and reliable.

Generally, it has been found that two generic optimisation techniques have been adopted in the design of microgrid systems: heuristic and classical techniques (Singh et al., 2016). The former technique is employed once long-term weather data for a given location is known but this is not always available, whilst the latter is typically employed in the design of microgrids if sufficient information of long-term weather data for the design location is available (Badwawi et al., 2015). Traditional or classical optimisation methods that are deployed in the microgrids design are an iterative approach, probabilistic approach, graphical construction methods, linear programming, trade-off method, and the least square method (Khan et al., 2018), (Rojas-Zerpa & Yusta, 2015). Various heuristic approaches have been employed in the techno-economic design optimisation of microgrid systems, such as genetic algorithm (GA), particle swarm optimisation (PSO), simulated annealing (SA), ant colony algorithms (ACA), bacterial foraging algorithm (BFO), artificial bee colony algorithm (ABC), biogeography-based optimisation (BBO), and artificial neural networks (ANN) (Bernal-Agustín et al., 2006; Cristóbal-Monreal & Dufo-López, 2016; Diaf et al., 2008; Khan et al., 2018; Olatomiwa et al., 2016; Singh et al., 2016). Erdinc and Uzunoglu (Erdinc & Uzunoglu, 2012) elaborate various heuristic optimisation techniques reported in the literature that contribute significantly to size hybrid microgrid systems, such as GA, PSO, SA.

Numerous studies have been extensively investigated in the literature to design microgrid systems for remote regions over the world. Traditionally, developing mathematical models of each subsystem and subsequently applying optimisation methods to size the entire system is adopted to design microgrid systems. In this regard, Halabi and Mekhilef (Halabi & Mekhilef, 2018) summarised the commonly used techniques in optimising HRES. Petrescu et al. (Petrescu et al., 2010) have investigated an optimisation method of a solar Stirling engine (SE) power plant to supply the required electrical energy demand for residential buildings using two sources, which are the parabolic dish mirror and the hydrogen/oxygen fuel cell. In particular, an extensive review of optimisation methods employed in the design of hybrid solar-wind systems has been performed but, in particular, the Photovoltaic (PV)/wind system has been overlooked in (Singh et al., 2016), (Badwawi et al., 2015). To obtain more reliability, a tri-hybridisation was implemented by Su Guo et al. (Guo et al., 2020). They proposed a new hybrid PV/Wind/thermal energy storage (TES) power system with an electric heater. The PSO algorithm was utilised to minimise the levelised cost of electricity (LCOE) and maximise the utilisation rate of transmission channels. In addition, Solar energy-driven multigeneration systems coupled with other renewable energies have been investigated comprehensively in Ref. (Mohammadi et al., 2020). They recommended, in the future, an investigation for such as the optimisation of solar energy-driven multigeneration systems.

For the hybrid systems that consist of concentrated solar power (CSP) and wind, there have been several attempts to optimise the hybrid CSP/wind system with the aim of minimising the power supply curtailment as the wind and solar energy usually do not peak simultaneously. To illustrate this isue, Yang et al. (Y. Yang et al., 2018) proposed a new hybrid system that includes CSP/wind/electric heater being employed with TES. This hybrid system is designed to optimise the profit under technical limitations as a mixed-integer linear programming problem. The proposed method has substantially reduced the wind curtailment by more than 90% over 151 days. Zeyu Ding et al. (Ding et al., 2019) have developed an optimisation technique based on a PSO algorithm to find the optimal design of the hybrid CSP/wind system coupled to TES. Such CSP/wind hybridisations are also seen in a recent study in the literature, Keyif et al. (Keyif et al., 2020). Keyif (Keyif et al., 2020) performed a non-linear optimisation model measuring the critical component investment costs and operational flexibility in the plant configuration.

The GA method is widely used in microgrid scheduling optimisation to investigate the optimum operating parameters. It is essential to combine the entire simulation model with a suitable optimisation method. Yang Hongxing et al. (H. Yang et al., 2009), (H. Yang et al., 2008) introduced a multi-objective GA method for identifying the stand-alone hybrid PV/wind system optimum configuration with the lowest cost based on the power supply probability (LPSP) and the annualised cost of the system (ACS). This developed model was implemented to provide electricity for a telecommunication relay station along the southeast coast of China. Similarly, Bilal et al. (Ould Bilal et al., 2010) have adopted two principles, namely the minimisation of ACS and LPSP with the use of GA on the northern coast of Potou, Senegal. Koutroulis et al. (Koutroulis et al., 2006) presented a minimum cost objective optimisation-based GA methodology for the optimal sizing of autonomous PV/wind systems to supply power for a residential household. For desalination purposes, Koutroulis and Kolokotsa (Koutroulis & Kolokotsa, 2010) have applied a GA methodology based on the total cost function minimisation for the optimal sizing of the PV/wind generator. Daming Xu et al. (Xu et al., 2005) investigated the GA approach of the sizing stand-alone hybrid PV/wind power systems. The objective of sizing these systems is to reduce the total capital cost, subject to the constraint of the LPSP. Bakir and Kulaksiz (Bakir & Kulaksiz, 2020) optimised the gain parameters of four PI controllers for the hybrid microgrid PV/wind system, which was modelled in MATLAB/Simulink® to examine the voltage profiles at the output. Two optimal sizing algorithms are used in the analyses are the Bacteria Foraging Algorithm (BFA) and GA.

According to Tafreshi et al. (Tafreshi et al., 2010), a GA method was also developed in the MATLAB® toolbox to find the optimum configuration for the hybrid PV/wind/biogas system. Furthermore, Kalantar and Mousavi (Kalantar & Mousavi G., 2010) have performed a GA method based on an economic analysis, i.e. ACS for decentralised the hybrid PV/ wind/microturbine/lead-acid battery storage system. Lagorse et al. (Lagorse et al., 2009) carried out the optimal sizing method for the multisource tri-hybrid PV/wind/fuel cell using GA based on the LCOE and meteorological features of the installed region and the consumption behaviour.

Other studies have been conducted by using GA to examine the reliability and dispatchability of a hybrid PV plant with a CSP plant. Starke et al. (Starke et al., 2018) have implemented a multi-objective optimisation approach based on the GA for evaluating the optimal design for hybrid CSP, including a central receiver system and parabolic trough collectors, and PV plants in Chile. The three objective functions were considered in this analysis: LCOE, overall investment and capacity factor. Moreover, four variables were adopted in terms of the design variables, namely: the solar field size, thermal storage capacity, PV power ratio and PV tilt angle. In addition, Liu et al. (Liu et al., 2019) utilised GA-PSO to obtain a minimised LCOE of the hybrid CSP-PV employing TES.

Based on the literature review, it is clear that there exists a lack in the literature of studies dealing with the optimisation analysis of the CPSD-SE/HWT integrated solution. To fill this knowledge gap, in this work, a concentrated parabolic solar dish Stirling engine (CPSD-SE) and a horizontal axis wind turbine (HWT) are integrated to generate power for a low to medium scale microgrid application. The predicted power that is generated by the system is in the range of 100 kWe and 1500 kWe, and the system performance throughout one year has been investigated dynamically via rigorous modelling. In addition, a techno-economic sensitivity analysis has been carried out to study the performance of the integrated hybrid system under the meteorological data for the city of Mafraq, Jordan using MATLAB/Simulink®. The main aim of the study is to carry out a post-design analysis of the new hybrid CPSD-SE/HWT system and calculate the generated power and efficiency. Furthermore, a multi-objective optimisation-based GA approach has been applied in which the $LCOE_{tot}$ and the energy efficiency of the system are simultaneously optimised. Optimal configuration and operating conditions in dispatch strategies are discussed in this work. Therefore, the main contribution of this work is to optimise the new hybrid CPSD-SE/HWT for power generation.

METHODOLOGY AND PROCEDURE

In this work, the performance of the system based on the operating conditions is considered in Mafraq, Jordan as a case study. The data for the study region in Jordan is provided by the Solargis™ satellite-driven data. In the performance model, the efficiency and the generated power of the existing system are measured depending on the predesign analysis of a published study (Shboul et al., 2021a). Further, a battery bank has been used as a recovery source of power to overcome the fluctuations in the solar and wind energy generation. The batteries are employed under the control of environmental operating conditions. CO_2 is used as a primary working gas in the SE and the predicted generated power is in the range of 100 kWe and 1500 kWe.

In general, the performance modelling and optimisation of the CPSD-SE/HWT using MATLAB/Simulink® is used by implementing the following steps:

- Specify the input and outputs variables of each sub-system as well as the assumptions that have been considered in this work. Table 1 shows the input and outputs variables of the model as well as the assumptions that have been considered in this work.
- The overall mathematical model of each unit has been carried out by implementing the fundamental thermodynamic energy balance equations that govern the operation of each investigated technology. The mathematical model of the integrated system is presented in Appendices 1-3.
- The models have been applied and solved in the MATLAB/Simulink® software based on the operating conditions, namely; the global solar radiation (GSR) and the average wind speed limit (AWS).
- The simulation results obtained by the proposed dynamic model of each sub-system is validated by comparing with the findings of previous related studies in the literature.
- To test the developed model and measure the dynamic performance of the system, the model has been implemented in Mafraq, Jordan, and the meteorological data is obtained from the Solargis™ toolbox.
- The multi-objective optimisation using GA methodology will be performed using Multi-objective GA Solver, which is built on the optimisation tool. The stepwise procedures for implementation of the GA optimisation in the MATLAB/Simulink® is shown in Figure 2.

Table 1. Data information related to the proposed system units

CPSD-SE							
Input parameters			**Output parameters**		**Assumptions**		
Description	**Value**	**Unit**	**Description**	**Unit**	**Description**	**Value**	**Unit**
Dish diameter	11	m	Top temperature	°C	Ambient temperature	25	°C
Receiver diameter	0.3	m	Engine efficiency	%	Atmospheric pressure	1.0132	bar
Number of dishes	60	-	Total efficiency	%	Receiver efficiency	80	%
working gas	CO_2		Engine and total powers	kWe	Solar flux limit	500-1000	W/m^2
Rim angle	37	degree	Compression ratio	-	Operating hours	10	h
Engine piston diameter	5.5	cm	Pressure ratio	-			
Piston stroke	5	cm	Mean effective pressure,	bar			
Engine speed	1800	rpm	Top temperature	°C			
Number of cylinders	4	-	Engine efficiency	%			
Generator efficiency	95	%					
Mirrors efficiency	97	%					
HWT							
Input parameters			**Output parameters**		**Assumptions**		

Description	Value	Unit	Description	Unit	Description	Value	Unit
Air speed ratio	0.35	-	Wind speed at blades	m/s	Ambient temperature	25	°C
Rotor diameter	47	m	Power coefficient		Atmospheric pressure	1.0132	bar
Number of modules	15	-	Wind power	kW	Wind speed limit	1.5-25	m/s
Generator efficiency	97	%	Mechanical power	kW			
Rotational loss	10.1-12	%	Generator power	kWe			
Power factor lag	0.9	-	Total farm power	kWe			
Battery bank							
Input parameters			**Output parameters**		**Assumptions**		
Description	**Value**	**Unit**	**Description**	**Unit**	**Description**	**Value**	**Unit**
Depth of discharge	0.8	-	Total power	kWe	Operating hours	24	h
Battery voltage	80	V	Battery storage	kWh	Load voltage	200	V
Battery current	10	A			Number of cloudy days	2	day
Battery Efficiency	75	%					
Number of batteries	1900	-					

Figure 2. The GA implementation steps in MATLAB/Simulink®.

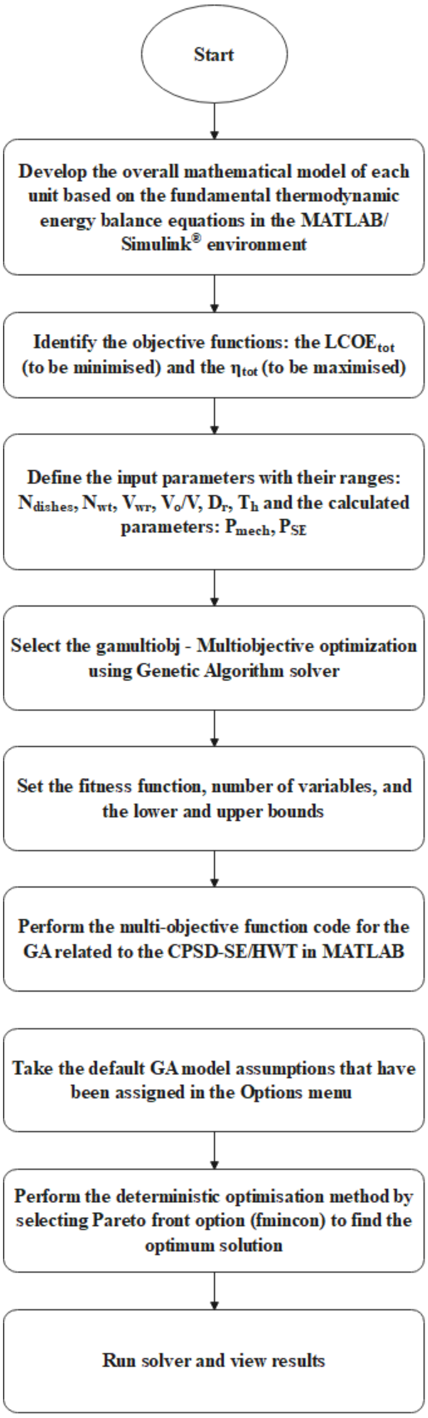

Site Location

The CPSD-SE system has economic feasibilities only for locations with direct normal irradiation (DNI) values higher than 5.5 kWh/m^2/day or 2000 kWh/m^2/year (Hirbodi et al., 2020). Jordan with an estimated average DNI of 2700 kWh/m^2 and approximately 300 clear sunny days per annum with 3311 hours and this is one of the most appropriate regions for the installation of CPSD-SE plants in the MENA region (The Middle East and North Africa). In addition, Jordan has a high annual average wind speed and this is higher than 7 m/s in some locations (with highs of 10 m/s) (H. H. Ali et al., 2020; Shboul et al., 2021). Consequently, the hybrid CPSD-SE/HWT is a suitable option for electricity production in Jordan. As shown in Figure 3, the northern region of Jordan, such as Mafraq with a daily average of DNI between 6.54 and 7.29 kWh/m^2 and an annual average wind speed of 4.72 m/s, has abundant wind speed and solar irradiations (*Global Solar Atlas*, 2020; *Global Wind Atlas*, 2020). Further, based on the study of Shboul et al. (Shboul et al., 2021), the city of Mafraq is one of the best regions in Jordan for exploiting the wind and solar potential as well as deploying hybrid CSP and wind plants. Thus, the city of Mafraq with latitude and longitude of 32.2^o N and 36.84^o E, respectively, has been selected as the case study location to investigate the stand-alone hybrid CPSD-SE/HWT plant in this research work.

Meteorological Data

In general, the climate conditions have a considerable influence on the performance and operation of microgrid power plants. The essential meteorological parameters to simulate the CPSD-SE/HWT plants in the adopted location by the MATLAB/Simulink® software are solar irradiation, wind speed, air temperature, relative humidity, and atmospheric pressure. In this study, these data were obtained from a newly developed ANN forecasting model for solar radiation and wind speed prediction based on the Solargis™ data (Shboul et al., 2021). This highly accurate model (error less than 3%) covers a wide time span of 20 years, and they have been validated to check the reliability and avoid errors in the results. The validated data have been used as input parameters in the MATLAB/Simulink® software.

Figure 3. Wind speed and DNI distribution in Mafraq (Global Solar Atlas, 2020; Global Wind Atlas, 2020).

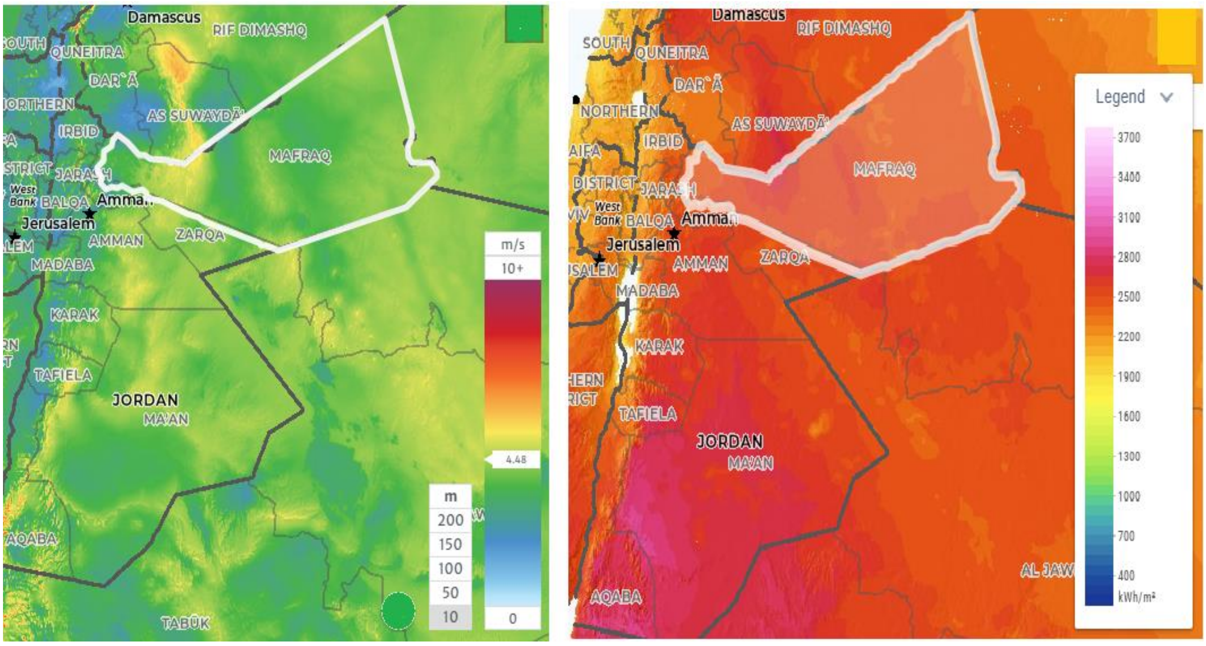

The monthly average of the meteorological data of Mafraq, including solar radiation, wind speed, air temperature, relative humidity, and atmospheric pressure, is indicated in Figures 4 and 5. As shown in Figure 4-a, the estimated solar data are the global horizontal irradiation (GHI), the DNI, and the diffuse horizontal irradiance (DIF). According to Figure 4-a, b, Mafraq city has the highest value of solar radiation (DNI and GHI) and wind speed and these occur in June and July, respectively. Also, it shows the lowest values of solar radiation (DNI and GHI) and the wind speed occur in January and December, respectively. In addition, the DIF meets its maximum and minimum values in June and December, respectively.

Figure 4. Monthly average data of (a) solar radiation and (b) wind speed.

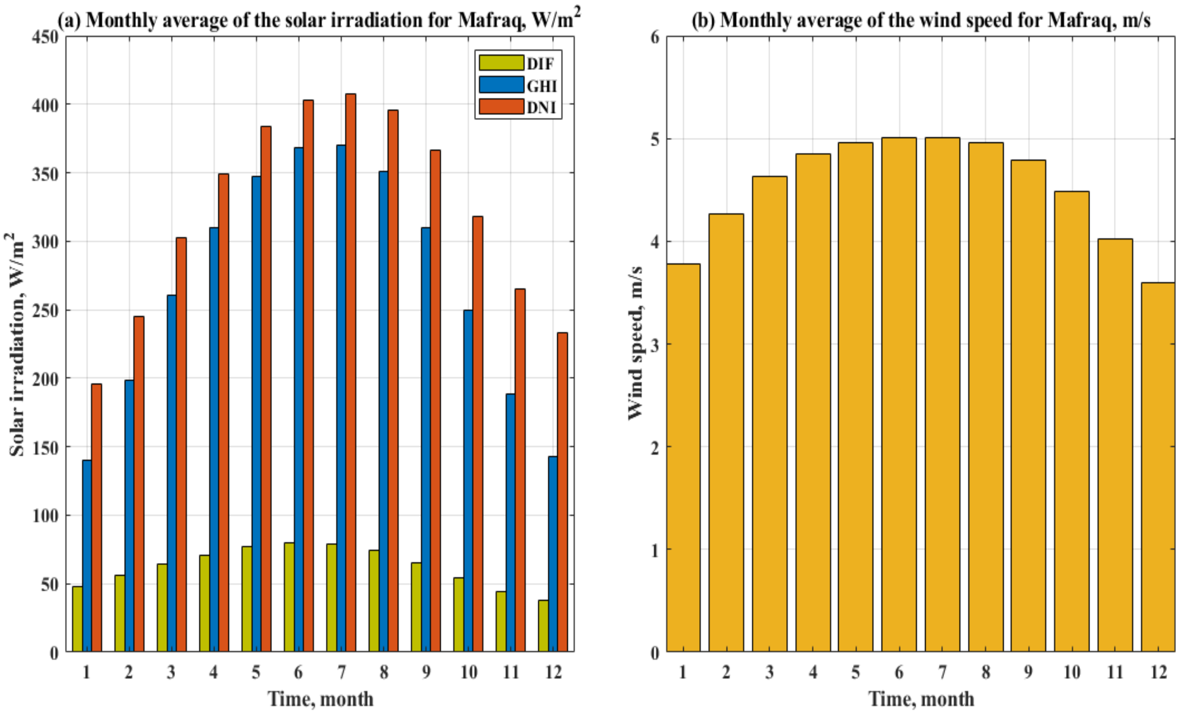

Based on Figure 5-a, the maximum and minimum values of the air temperature are in July and January, respectively. Figures. 5-b and 5-c illustrate that the relative humidity and atmospheric pressure reach their maximum values in December and January and their minimum values in June and July.

Figure 5. Monthly average of the meteorological data for Mafraq, Jordan.

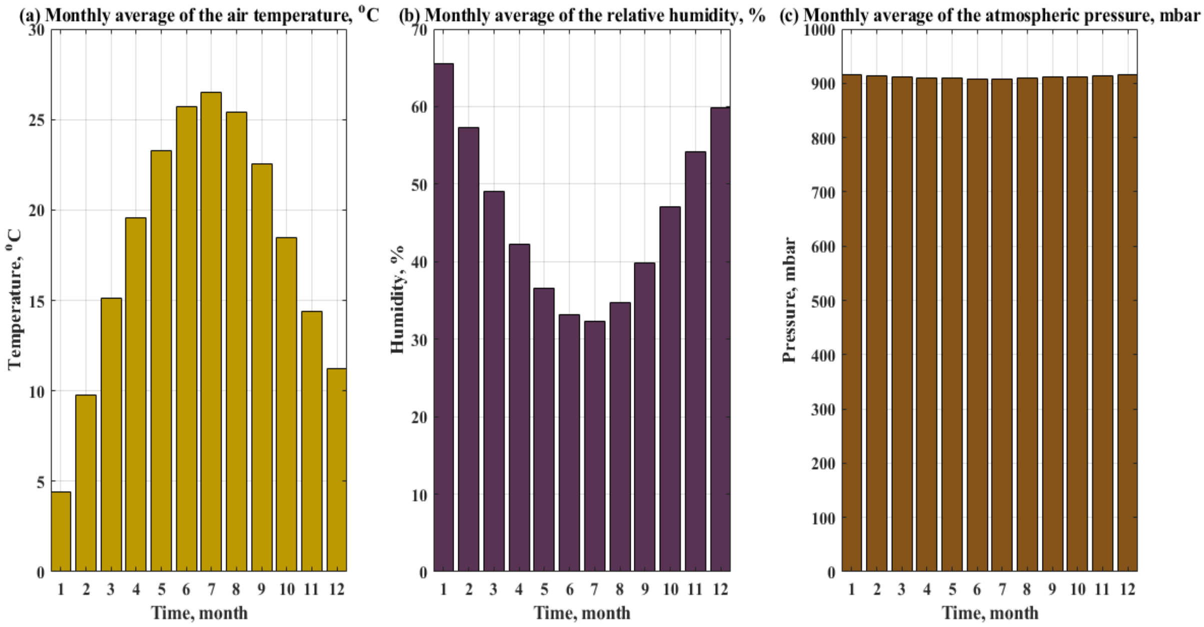

In order to determine the hourly meteorological variables, a signal builder has been developed as the input parameter to the ANN model in the MATLAB/Simulink®. For this purpose, it is primarily used to analyse the CPSD-SE/HWT plant output variations each hour throughout one year, as shown in Figure 6.

Figure 6. Data signal entry for one year in the ANN model – adapted from (Shboul et al., 2021).

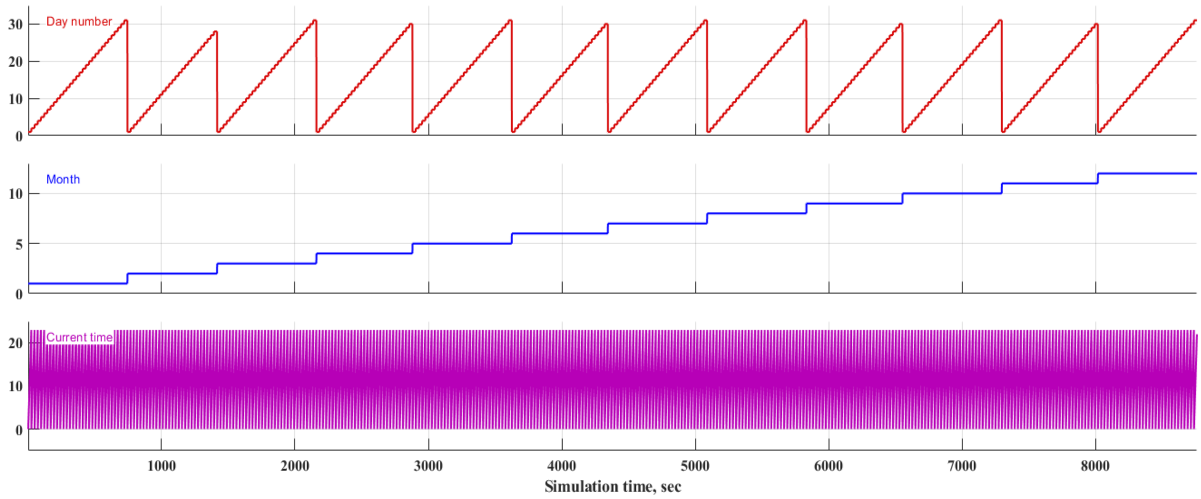

Figure 7-a shows the hourly solar radiation (GHI, DNI, and DIF) and the wind speed recorded for the Mafraq City over one year. The annual solar irradiance for GHI, DNI, and DIF at the site varies in the range of 200 to 1015 W/m^2, 300 to 875 W/m^2, and 152 to 189 W/m^2, respectively. It should be noted that the annual GHI is close to the global maximum of GHI. Therefore, this can be traced back to the coordinates of the location in the Sunbelt region. The hourly wind speed recorded at a height of 10 m for the selected location is shown in Figure 7-b. According to Figure 7-b, the average wind speed at the site is approximately between 2.3 m/s and 5.8 m/s and this wind energy potential is sufficient to generate a reasonable amount of electricity.

Figure 7. (a) Hourly GHI, DNI, and DIF and (b) average of hourly wind speed during a year for Mafraq, Jordan.

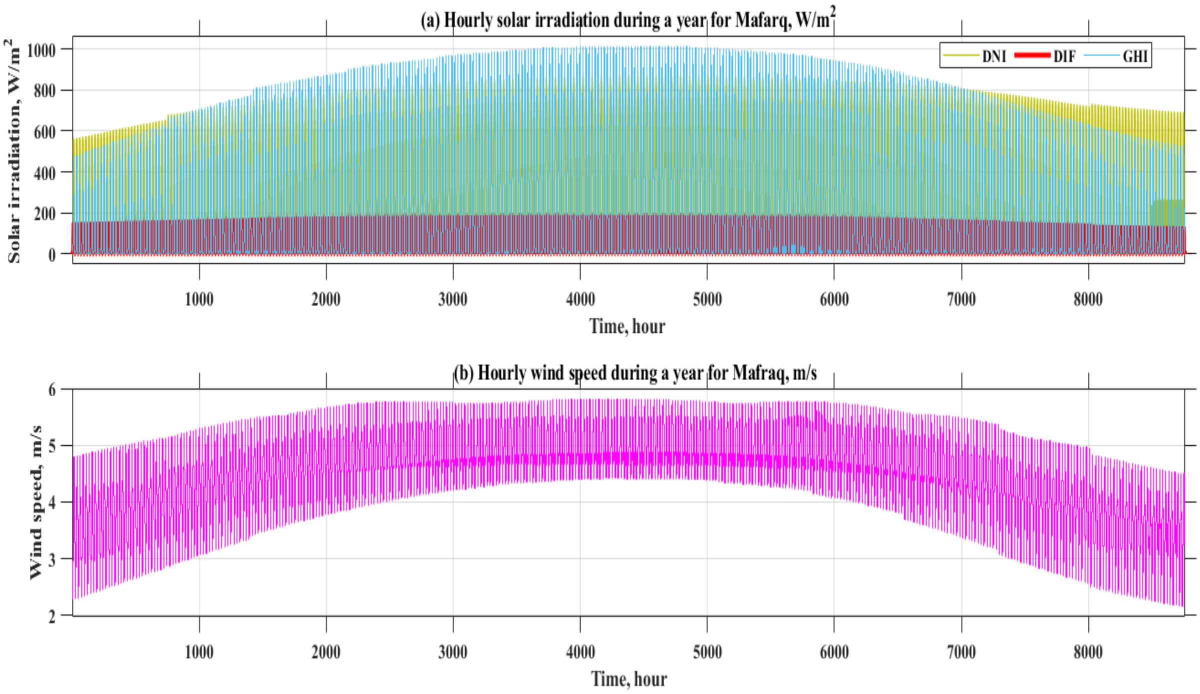

The ambient temperature, relative humidity, and air pressure are critical climatic parameters and these have a direct effect on the characteristics of the CPSD-SE system and power load. Figures 8-a, b, and c demonstrate the annual profile of hourly meteorological parameters for Mafraq City. Figures 8-a to 8-c show that the mean temperature, humidity, pressure of Mafraq City varies from less than -3.2oC, 17.73%, and 907.3 mbar by more than 33.3ºC, 83.4%, and 916.5 mbar, respectively.

Figure 8. Hourly average of the meteorological data throughout the year for Mafraq, Jordan.

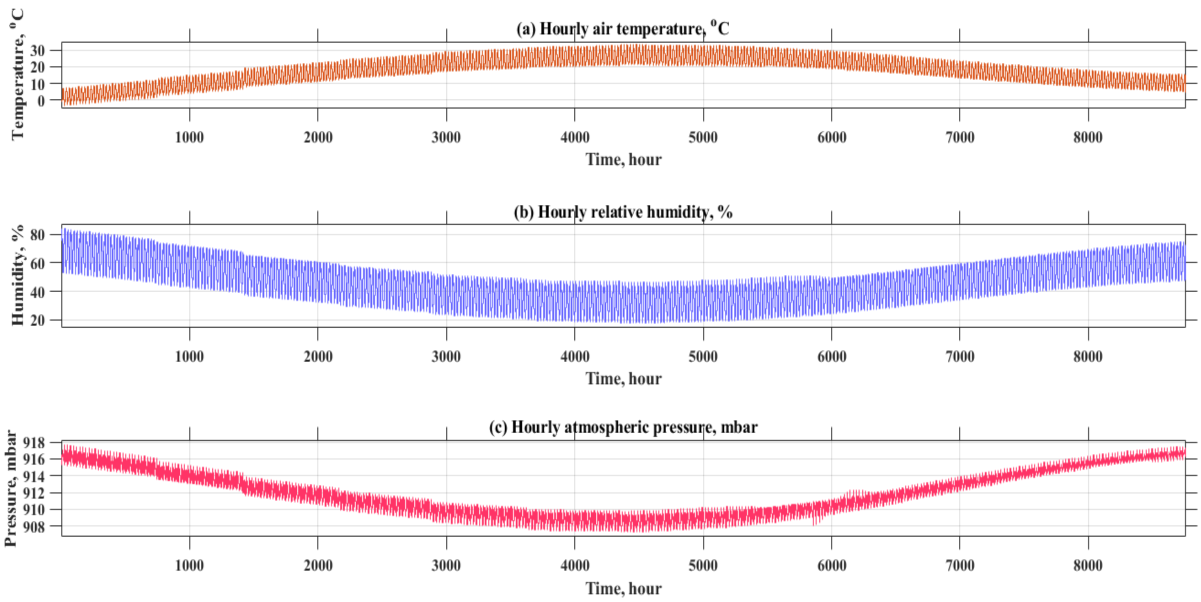

Electric Load Data

The hourly electrical load of the selected case study represents the load power variation for typical residential buildings in remote regions. The load demand was obtained at an hourly interval throughout the year. Also, the load has been estimated using the random fluctuation mode based on the computational code to approximate real-time operation. The annual and monthly fluctuations of the hourly load consumption is depicted in Figures 9 and 10, respectively. To illustrate this model, an array of random floating-point numbers that are drawn from a uniform distribution has been created. By default, "*rand*" returns normalized values (between 0 and 1) that are drawn from a uniform distribution. To change the range of the distribution to a new range, (a, b), multiply each value by the width of the new range, (b – a) and then shift every value by a. To utilise this proceedure, it should initialise the random number generator to make the results repeatable with equal probability. In this case, the random number is denoted *n*, which is the number of hours either in the month or during the year. To illustrate, the "*n*" values in the month are 672, 720, and 744, which comes from the multiplication of 24 hours by the number of days in that month and thus indicating the total number of hours in a month. Subsequently, the monthly average of the hourly electrical load would be calculated by multiplying the random hours' number with the power range from 100 to 1500 kWe. Similarly, the hourly electrical load during a year could be calculated by multiplying the adopted power range with 8760 random hours. Appendix 6 shows the numerical code that was used to estimate the electrical load.

Figure 9. Hourly electrical load for the addressed location during a year.

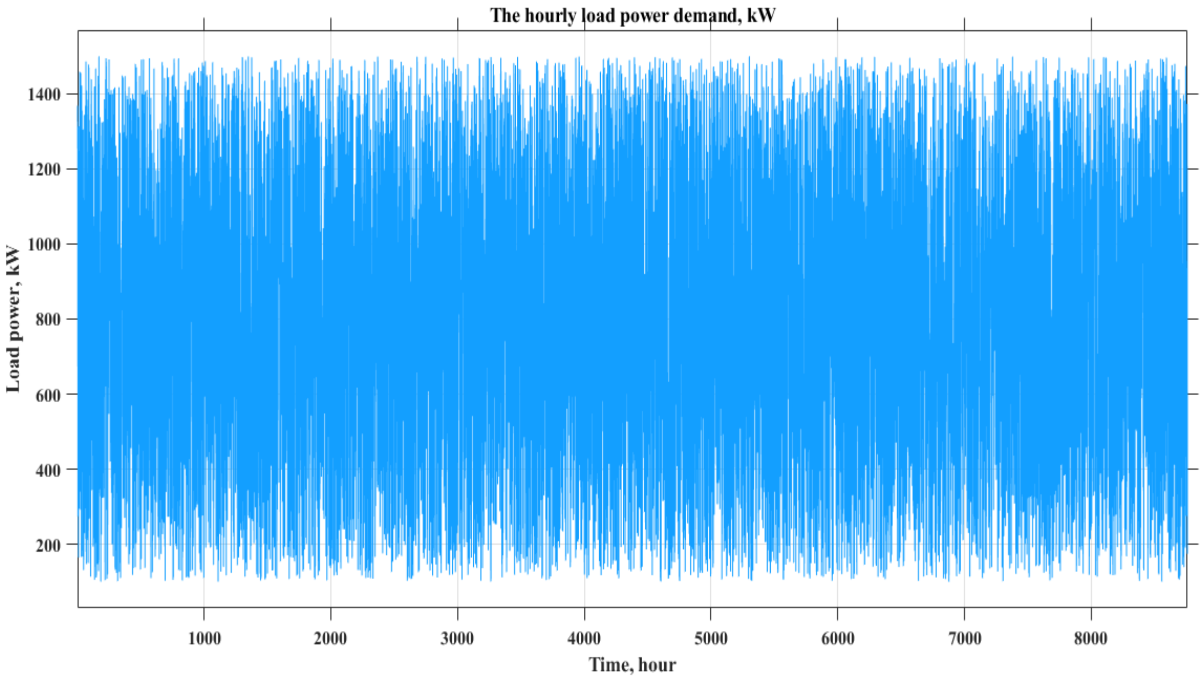

Figure 10. Monthly average of the hourly electrical load for the addressed location.

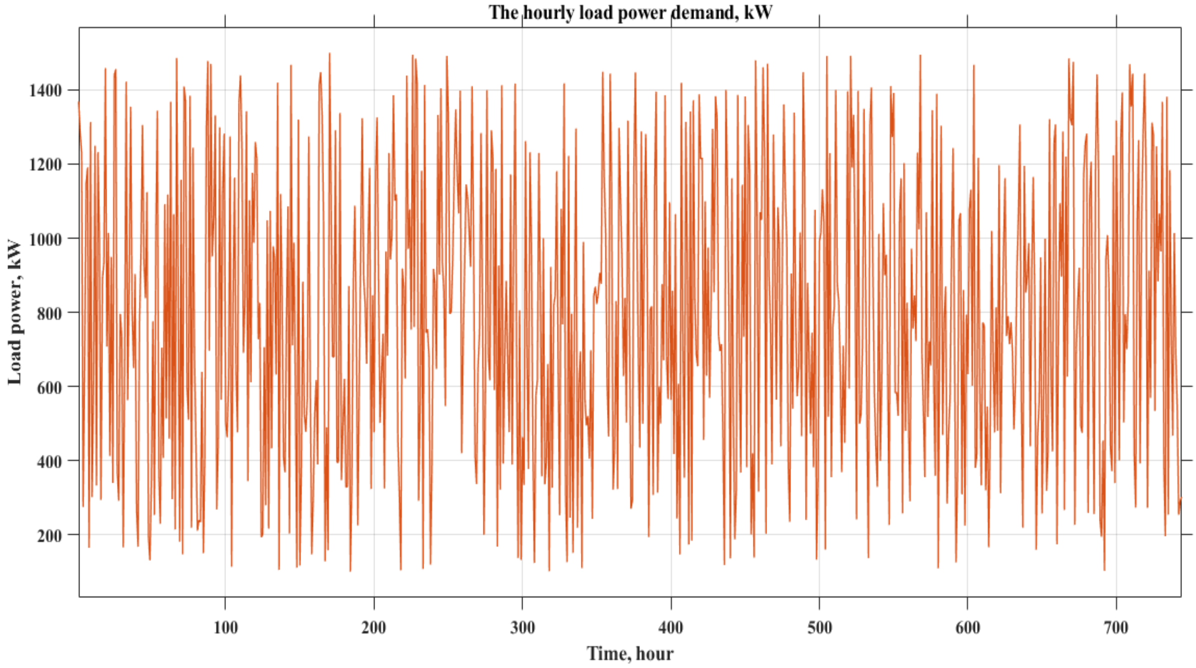

The Proposed CPSD-SE/HWT System

The designed system is suitable for power generation on a residential scale of arid and semi-arid regions. Figure 11 shows a schematic diagram of the proposed hybrid CPSD-SE/HWT stand-alone microgrid power system for the residential buildings described herein. The system main units are as follows:

- ANN solar/wind forecasting model.
- CPSD-SE as a prime power source.
- HWT as a recovery unit.
- Battery bank as an energy storage system.
- Control unit for power disruption & application load.

Figure 11. Schematic diagram of the proposed new hybrid CPSD-SE/HWT system – adapted from (Shboul et al., 2021).

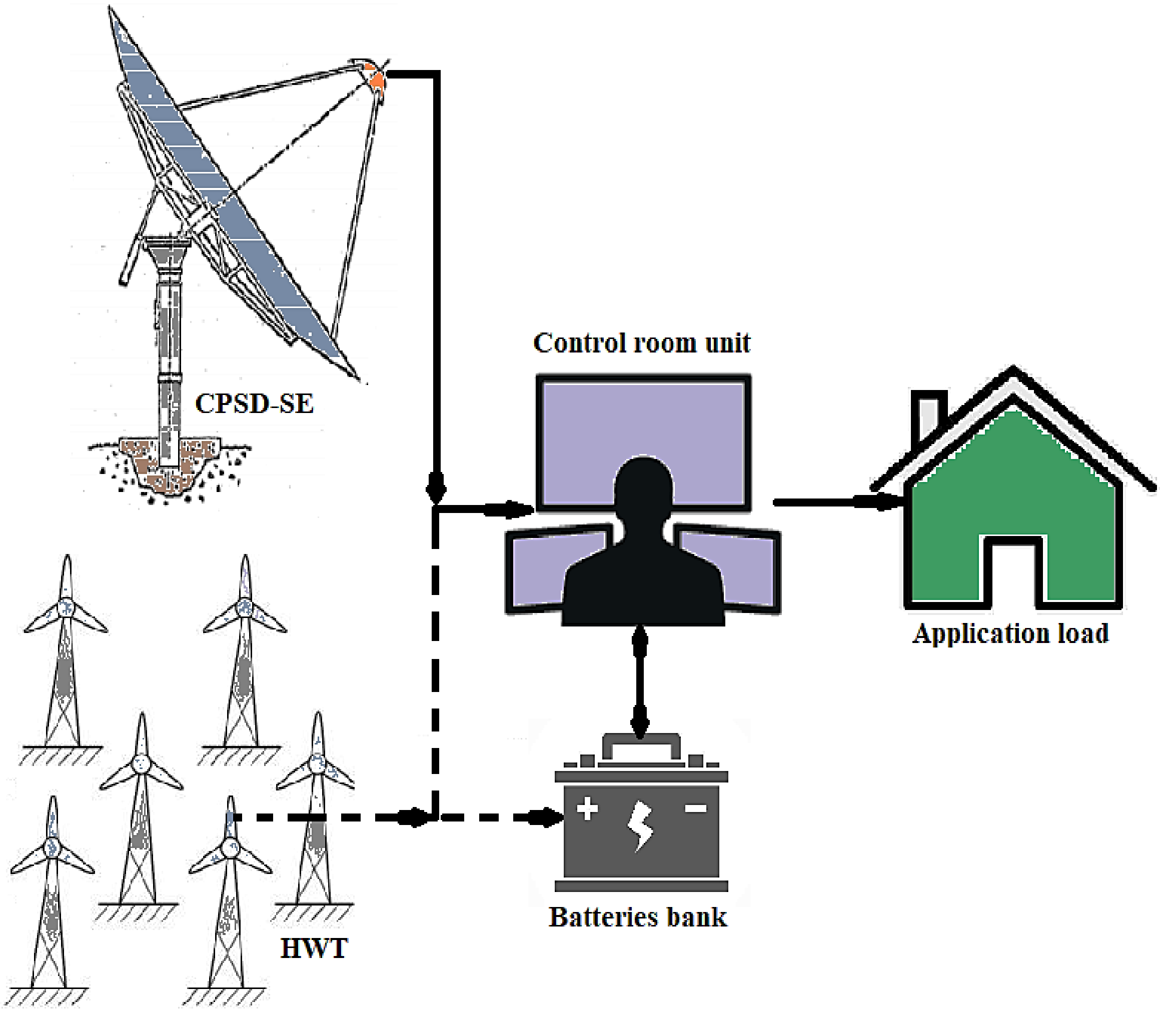

The CPSD-SE will serve as the main source of power generation, while the batteries bank and HWT will provide backup power in case that the primary source of electricity becomes unavailable. This maintains power production continuity. The CPSD-SE system consists of a collection of parabolic dish collectors and a power conversion unit comprised of a Stirling engine (SE), a thermal receiver and an alternator. The primary characteristic that differentiates the CPSD-SE from other solar technologies, such as concentrated solar power (CSP) and photovoltaic (PV), is its capacity to directly convert solar radiation into electrical and thermal energy. In a typical CPSD-SE, three main forms of energy conversion are produced: solar, thermal, and electrical energy. Figure 12 shows the thermodynamic balance diagram of the CPSD-SE diagram (Zayed et al., 2020). In principle, the CPSD-SE mirrors reflect incident sunlight to a focal point on a thermal receiver (i.e., the SE's hot chamber), converting the concentrated radiation into thermal energy to generate heat at a high temperature. The absorbed heat is then transferred to the SE's working fluid via the heater driving an electric generator. In three different mechanisms, the receiver loses heat by conduction through its walls: convection to the surrounding air, radiation from the aperture opening to the atmosphere. In the absence of sunshine, the power demand is provided by the HWT. Moreover, the batteries are being discharged when the CPSD-SE and HWT cannot generate the electricity. To achieve optimum performance and optimum sizing, GA is used for that purpose.

Figure 12. Thermodynamic balance diagram of the CPSD-SE system (Zayed et al., 2020).

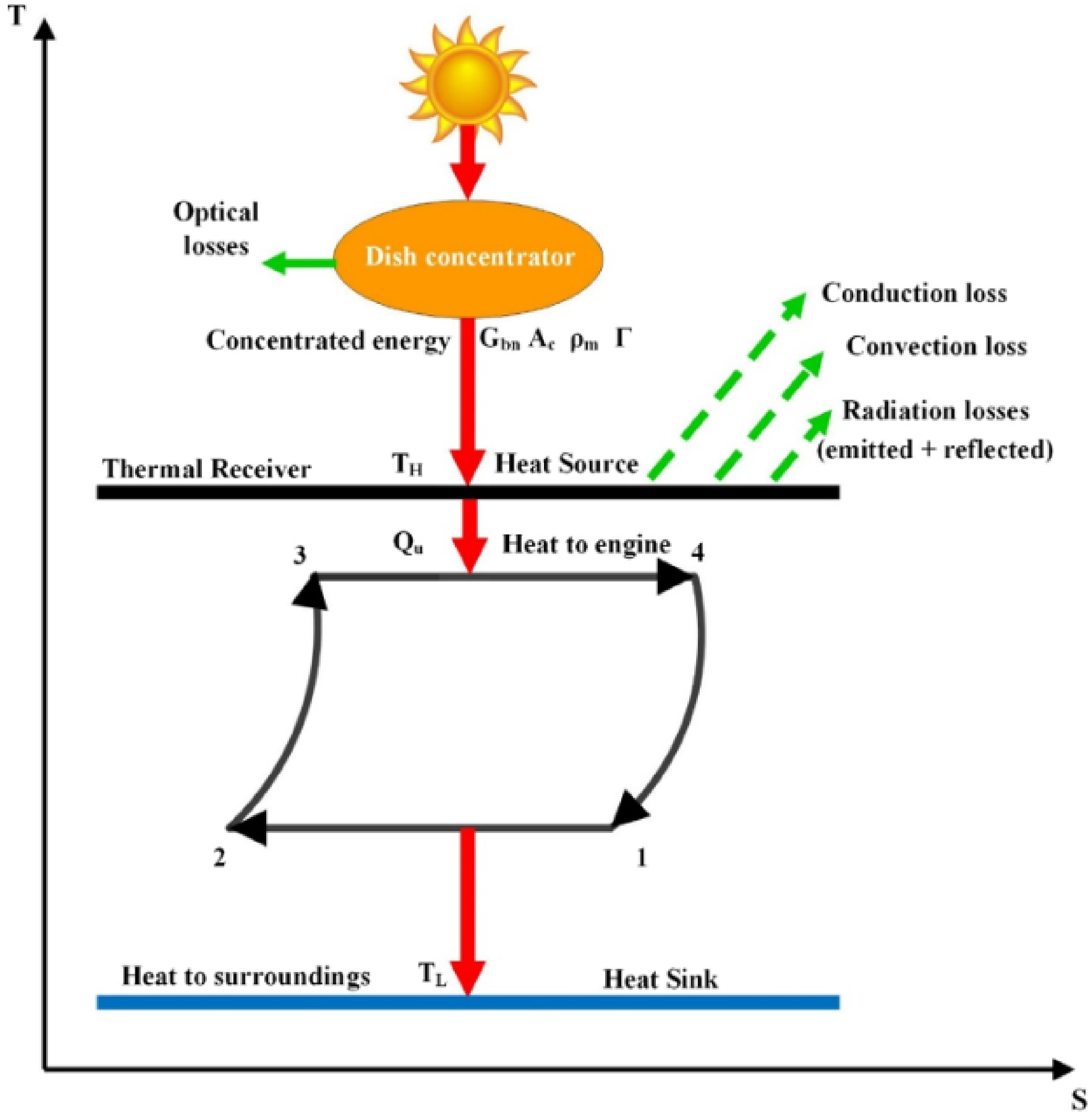

The ideal Stirling cycle is fundamentally composed of four processes; two isothermal and two isochoric processes as can be seen in Figure 13 (Yunus A. Çengel, 2015). These four processes are as follows:

i. 1-2 is an isothermal expansion process. The working fluid is expanded at constant temperature T_H, and after that heat, q_{in} is absorbed from the external heat source.

ii. 2-3 is an isochoric heat removal process. The working fluid releases heat is transferred through to the hot side of the engine. The temperature of the working fluid is gradually decreased and this causes a pressure drop.

iii. 3-4 is an isothermal compression process. The working fluid is compressed at constant temperature T_L, and then heat q_{out} is released to the heat sink.

iv. 4-1 is an isochoric heat addition process. The working fluid absorbs heat and this is transferred from the regenerator to the cold side of the engine. The temperature of the working fluid is gradually increased and this causes an increase in the pressure.

It should be noted that the amount of sunlight incident on the reflectors will be utilised exclusively for electricity generation, with no consideration given to thermal output. To summarise, the developed thermodynamic model based on energy balance was obtained by adopting the following assumptions:

- The heat lost by the receiver via conduction is disregarded.
- The optical heat loss is disregarded.
- The dissipated heat from the SE is disregarded.
- The receiver and generator efficiencies are given.

Figure 13. P-v and T-s diagram of the Stirling cycle (Yunus A. Çengel, 2015).

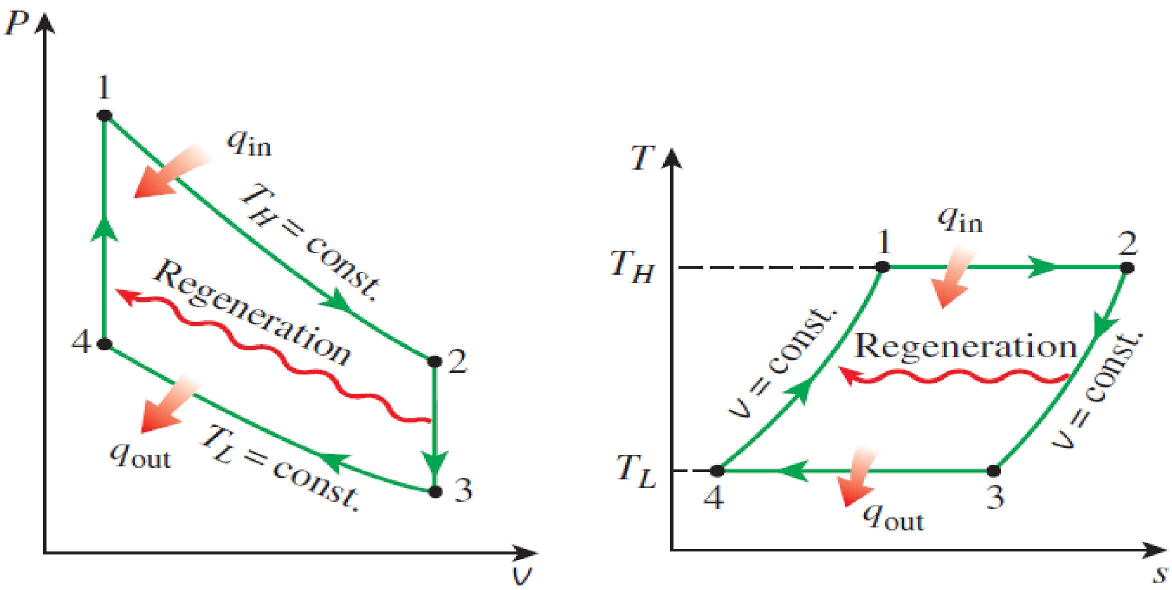

Simulation Tool Selection

In this research work, the MATLAB/Simulink® software is applied to perform the performance and optimisation analysis of the proposed hybrid CPSD-SE/HWT. The main reason for the selection of the MATLAB/Simulink®, for hybrid CPSD-SE/HWT modelling and optimisation purposes are: (i) it includes Simulink blocks (drag & drop ability) with appropriate connections based on the proposed design; (ii) each block contains a variety of MATLAB® command functions, and the system is solved iteratively; and (iii) the optimisation Toolbox™ is made up of multiple solvers for the optimisation techniques to minimise or maximise the objectives while satisfying the constraints. The friendly graphical user interface is powerful for setting up and running optimisation problems, including parameter estimation, component selection, and parameter tuning. This tool has numerous significant applications in the design optimisation, such as an energy management system and production planning. Accordingly, these features facilitate the user to be able to execute further calculations, such as sizing and economic calculations.

Economic Performance Analysis

The economic considerations are vital for assessing the competitiveness of the electricity production from power generation systems. The economic performance model is developed in the MATLAB/Simulink® using a set of correlations based on four economic indicators, namely the total levelised costs of energy, $LCOE_{tot}$, *$/kWh*, total hourly cost, THC_{tot}, $/h, annual electricity savings, *AES*, *$*, and the payback period, *year*. In this regard, the economic parameters of the CPSD-SE/HWT system, these were calculated using Eq. (1) to (4). The detailed cost analysis model that has been considered in this study and this is described in Appendix 4 (Shboul et al., 2021a). In this work, the batteries are being charged when the electricity production is in surplus from the CPSD-SE and HWT, while on the another hand, the batteries bank would deliver electricity to the application load when there is a shortage in the availability of wind and sunlight. Moreover, the key inputs comprise the following economic indicators: the plant lifetime, interest rate, power cost, variable operating cost and fixed charge rate. Consequently, the subsequent assumptions have been undertaken: plant lifetime is 25 years, the interest rate is 5%, variable operating cost for the solar dish and turbine are 0.06 $/kWh and 0, respectively, the fixed charge rate is 0.098, battery lifetime is 5 years, turbine power cost is 1628 $/kWe, battery cost is 100 $/unit, dish cost is 300 $/m^2, engine cost is 370 to 400 $/kWe, receiver cost is 185 $/kWe, and site cost is 2.2 $/m^2. Table 2 displays the economic assessment variables and assumptions. The $LCOE_{tot}$ is calculated using the following expression (Shboul et al., 2021a):

$$LCOE_{tot} = \frac{THC_{tot}}{Load\ factor \times\ P_{tot}} + VOC_{tot} \tag{1}$$

where THC_{tot} is the total hourly costs, $/h, VOC_{tot} is the total variable operating costs, $/kWh, P_{tot} is the total plant power, kWe and the load factor is 0.9.

The THC_{tot} is calculated as follows (Shboul et al., 2021a):

$$THC_{tot} = \frac{ATC_{tot}}{8760} \tag{2}$$

where ATC_{tot} represents the total annual cost of the power plant, $/y, including the annual cost of the batteries, HWT and CPSD-SE.

The AES can be determined according to the following expression (Saffari et al., 2018):

$$Electricity\ cost = LCOE_{tot} \times Annual\ electricity\ generated \tag{3}$$

where the annual electricity generated is in kWh.

The payback period is used to estimate the financial competitiveness, which can be calculated by the following equation (Wang et al., 2015):

$$Payback\ period = \frac{TCC_{tot}}{Electricity\ cost} \tag{4}$$

where TCC_{tot} is the total capital cost of the system units, $.

Table 2. Economic parameters for all units that have been considered in the cost analysis model.

Input economic parameters		
Parameter	**Value**	**Reference**
Interest rate, %	5	(Nafey et al., 2010)
Battery lifetime, year	5	(Nafey et al., 2010)
Plant lifetime, year	25	(Nafey et al., 2010)
Fixed charge rate	0.098	(SAM, 2021)
Electricity sale price, $/kWh	0.183	(Helioscsp, 2014)
Annual electricity generation, kWh	22.28	Present model
Direct costs		
Battery cost, $	100	(Shboul et al., 2021a)
Normalised capital cost of the wind turbines, $/kWe	1628	(Shboul et al., 2021a)
Stirling engine cost, $/kWe	370	(Shboul et al., 2021a)
Receiver cost, $/kWe	185	(Shboul et al., 2021a)
Dish concentrator cost, $/m^2	300	(Shboul et al., 2021a)
Indirect costs		
Site cost, $/m^2	2.2	(Shboul et al., 2021a)
Wind turbine cost-share, %	65	(Shboul et al., 2021a)
Construction cost share (civil works), %	16	(Shboul et al., 2021a)
Other capital cost-share, %	5	(Shboul et al., 2021a)
Construction, procurement, and engineering cost-share, %	16	(Shboul et al., 2021a)
Contingency cost-share, %	10	(Shboul et al., 2021a)
Other capital cost-share, %	3	(Shboul, et al., 2021a)
Variable operating costs		
Variable operating cost of the batteries, $/kWh	0.07	(Shboul et al., 2021a)
Variable operating cost of the wind turbines, $/kWh	0	(Shboul et al., 2021a)
Variable operating cost of the CPSD-SE, $/kWh	0.06	(Shboul et al., 2021a)

The Multi-objective GA Methodology

The GA is an optimisation technique known as the evolutionary algorithm used to solve complex, large-scale optimisation problems in various fields based on the mechanism of the natural selection process that mimics biological evolution. GAs search for the optimum solution from one of the candidate solutions that is an array of decision-variable values. These random solutions that are tested against the objective function are called a population. Each individual in the population is called a chromosome. Several populations evolve through successive iterations, namely the selection, crossover and mutation in a GA run and all of these populations are referred to as a generation. In general, with each newer generation, improved solutions (i.e., decision-variable values), which are nearer to the optimal solution than the preceding generation are formed. In the GA context, the set of alternative solutions (array of decision-variable values) is referred to as a chromosome, and each decision-variable value represent in the chromosome is designated by genes (Rani et al., 2013). The size of the population is the number of chromosomes present in a population. The GA mechanism is briefly outlined in Figure 14.

Figure 14. Flow diagram of the overall GA process (Dincer et al., 2017).

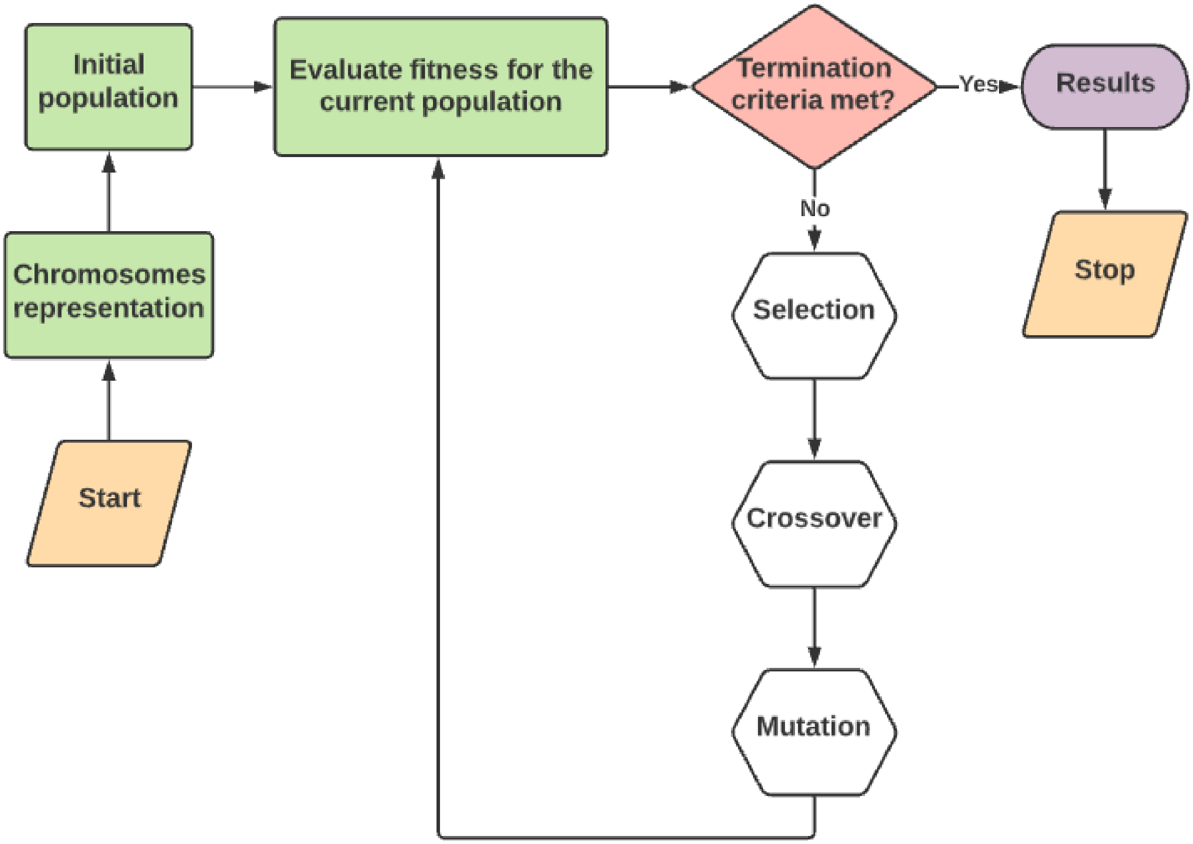

The GA offers a number of advantages over traditional optimisation techniques, which can be listed as follows:

- The GA can be used with continuous as well as discrete variables.
- The GA is capable of dealing with a high number of variables.
- The GA could deal with numerical, experimental, and analytical objective functions.
- The GA technique does not require derivative information.
- The GA would save the overall computational time.
- The GA used to solve stochastic optimisation problems that could be stuck to the optimum.

In this work, it is particularly important to assign the main multi-objective GA model criteria regarding the main process as shown in Figure 14. Generally, a multi-objective optimisation problem can either minimise or maximise the objective function. Unlike single-objective optimisation, multiple objectives are being implemented that require different constraints, all of the possible solutions must be accomplished at once, including the optimum one. A multi-objective optimisation problem can be formulated as follows (Dincer et al., 2017):

$$\text{Minimise/ maximise: } \{f_n(x) \qquad n = 1,2, \dots N$$

$$\text{Subject to: } \begin{cases} g_i(x) > 0 & j = 1,2, \dots J \\ h_k(x) = 0 & k = 1,2, \dots K \\ {x_i}^{(L)} \le x_i \le {x_i}^{(U)} & i = 1,2, \dots n \end{cases}$$

In this case, we need to the solve vector of the *n* decision variables or design parameters to find *x*, with one for each variable. The last set of constraints is called the variable bounds, which restrict the searching bound. Any solution exists inside a lower bound (${x_i}^{(L)}$) and upper bound (${x_i}^{(U)}$) of the decision variables.

Objective Functions

The main purpose of hybridising CPSD-SE/HWT is to minimise the overall plant costs and achieve a higher average overall annual plant efficiency (η_{tot}), thus increasing the competitiveness of solar/wind electricity. In this context, the multi-objective GA optimisation procedure for the CPSD-SE/HWT power plant proposed herein considers two objective functions: the $LCOE_{tot}$ (to be minimised) and the η_{tot} (to be maximised). The multi-objective function code for the GA related to the CPSD-SE/HWT is performed as presented in Appendix 5.

Optimisation Framework

For the hybrid CPSD-SE/HWT, the model will consider 6 main inputs and 2 calculated parameters (intermediate inputs) for the target optimisation of two outputs. As mentioned earlier in section 2.5.1, the main target of this model is to minimise the levelised cost of electricity, $LCOE_{tot}$, \$/kWh and maximise the average overall annual efficiency, η_{tot}, %, as illustrated in Eqs. (1) and (5) (Shboul et al., 2021a). The detailed multi-objective GA model that has been considered in this study is presented in Appendix 5. The main inputs of the optimisation function are the number of dish units, N_{dishes}, number of wind turbines, N_{wt}, average wind speed, V_{wr}, m/s, air speed ratio, V_o/V, rotor diameter, D_r, *m*, and top cycle temperature, T_h, ^oC. The calculated parameters are the mechanical power, P_{mech}, *kWe,* Stirling engine power, P_{SE}, *kWe*. The model assumed that the number of batteries is 1900, collector area, A_c, m^2, the normalised capital cost of the wind turbine, *\$/kW,* solar radiation, *DNI*, W/m^2 and lower cycle temperature, T_l, ^oC are equal to 95 m^2, 1628 \$/kW, 875W/m^2 and 25 ^{o}C, respectively. Also, the generator efficiency, η_{gen}, receiver efficiency, η_r, and mirror efficiency, η_c, are equal to 95%, 97%, and

80%, respectively. Moreover, the model assumed that air pressure, P_{air}, bar, is 1.0132, and site elevation, H_s, m is 10. Table 3 summarises the parameters related to the optimisation model.

$$\eta_{tot} = \frac{P_{tot} \times 1000}{\left(I_s \times A_{c,tot}\right) + \left(P_w \times N_{wt}\right)} \tag{5}$$

where P_{tot} is the total plant power, *kWe* (P_{mech}+P_{SE}), I_s is the solar irradiation, W/m^2 (equals to the DNI), $A_{c,tot}$ is the total plant power of the CPSD-SE, *kW*, P_w is the wind power, *W* and N_{wt} is the number of wind turbines.

Table 3. The developed GA multi-objective functions related to the entire model optimisation

Input parameters and ranges			
Parameter	**Symbol**	**Unit**	**Range**
Number of dishes	N_{dishes}	#	20-80
Number of wind turbines	N_{wt}	#	1-20
Average wind speed	V_{wr}	m/s	2-6
Air speed ratio	V_o/V	-	0.2-0.6
Rotor diameter	D_r	m	60-140
Top cycle temperature	T_h	ºC	200-800
Calculated parameters			
Wind turbine mechanical power	P_{mech}	kWe	1.77-1170.33
Stirling engine power	P_{SE}	kWe	11.34-22.13
Outputs			
Total levelised cost of energy	$LCOE_{tot}$	$/kWh	
Average overall annual efficiency	η_{tot}	%	

SIMULATION RESULTS AND DISCUSSION

In this part of the chapter, first, the validation of each system unit is conducted individually via the comparison with actual power plants and both theoretical and actual published works. Also, the dynamic performance analysis is performed to obtain the energy yield and efficiency of the CPSD-SE/HWT via the MATLAB/Simulink® environment. Steady-state conditions are primarily applied to all runs and the design specifications and operating conditions, as presented in Table 1, are entered into the model. The MATLAB/Simulink® can be considered an ideal platform for an economic potential assessment of the plant. Then, a sensitivity analysis of the key parameters, that affect the performance of the system components, is carried out. Finally, according to the GA method, the optimum energy system is identified based on multi-objective functions.

Mathematical Model Validation

The simulation results, estimated in this analysis for the developed hybrid CPSD-SE/HWT model in MATLAB/Simulink®, are compared and validated with both the simulated published data and actual power plants. Tables 4 and 7 provide a comparison of the findings evaluated from this study, other commercial models and published results, which indicates reasonable variations. Clearly, the results obtained from this research demonstrate that the MATLAB/Simulink® software is very reliable; consequently, it may be used to generate realistic findings in additional analyses in the discussion section by simulating the CPSD-SE and HWT and optimising the developed model.

As with other models, the model validation is carried out to confirm the model adequacy by comparing the results of data sets provided either independently or experimental, which align with the simulated scenario, to those estimated by the present model. Therefore, the operational model validation method is selected to determine whether the model findings agree with the observed data. Consequently, a deterministic model has been developed in this study using the dynamic programming methodology. Furthermore, two distinct aspects are taken into consideration during the model validation involving the input parameter and operating condition values and also the assumptions. To illustrate, the design specifications of the HWT and CPSD-SE then these are presented in Tables 4 and 6, respectively. In addition, two approaches are applied following the various attributes of the model, including theoretical results and real system measurements. Nevertheless, in practice, full validation of the entire model would be challenging, particularly whether the system is being modelled does not yet exist. In this work, the validation will focus on the output of each unit separately.

HWT Model Validation

The specifications of the selected HWT model (The Wind Power, 2020) are listed in Table 4 and is briefly described below. The simulation results obtained by the proposed dynamic model of the HWT system is validated by using results from other existing models, and the results from this model are compared with other types of commercial HWT models. These models include the GAMESA model in the Ma'an Part I wind farm in Ma'an, Jordan and the ENCORN model in the Feldheim wind farm in Germany (The Wind Power, 2020). The data is obtained by inputting the same geometrical design parameters and operating conditions. As shown in Table 5, the comparison reveals an excellent agreement between the developed model and the selected wind farms. It is shown that the output power per HWT unit of the developed model has errors of approximately 0.55% and 1.99%, compared to the Ma'an Part 1 and Feldheim wind farms, respectively.

Table 4. Specifications of the selected models

Description	**Wind farm**	**Ma'an Part 1**	**Feldheim**
General data	Country/zone	Jordan/Ma'an	Germany
	Manufacturer	GAMESA	ENCORN
	Model	G97/2000	E115 3.000
	Number of Turbines	33	3

	Total nominal power	66000 kW	9000 kW
Operating data	Rated power	2000 kW	3000 kW
	Cut-in wind speed	3 m/s	2 m/s
	Rated wind speed	14 m/s	11.5 m/s
	Cut-out wind speed	25 m/s	25 m/s
Rotor	Rotor diameter	97 m	115.7 m
	Swept area	7390 m^2	10515.5 m^2
	Rotational speed	9.6-17.8 rpm	12.8 rpm
Generator	Generator efficiency	0.97	0.97
	load factor	0.95	0.95
Tower	Hub heights	78-120 m	92,135, and 149 m
Power curve	Wind speed	0-25 m/s	0-25 m/s
	Power coefficient	0.18	0.33

Table 5. Data validation results of the HWT model

Description	The developed model	Ma'an (Gamesa G97/2000)	Error (%)	The developed model	Feldheim (Encorn E115 3.000)	Error (%)
Module power	2011	2000	0.55	3000	3061	1.993
Hub height	121.3	120	1.083	149	144.6	3.043
Rotor swept area	7389.81	7390	0.00257	10515.5	10513.72	0.0169

CPSD-SE Model Validation

In this study, the proposed mathematical CPSD-SE model was developed using the MATLAB/Simulink® toolbox to carry out the performance analysis. Table 6 lists the geometrical and operating parameters of the CPSD-SE models used for validation. To validate, the simulation results of the present model then these results are compared with the findings of previous related studies from Refs. (v. Siva Reddy, 2012; Zayed et al., 2020) under the same operating conditions. The comparison shows that the same major parameters of the two models have an excellent agreement, as indicated in Table 7. For instance, the Stirling efficiency values have a percentage of deviation of approximately 4.98% and 16%, when compared with Refs. (v. Siva Reddy, 2012; Zayed et al., 2020), respectively. These deviations in the simulation results of the two different systems could be caused by adopting different parameters in the different modelling techniques. Overall, it can be concluded from the high validity of the obtained results that this developed model is a reliable tool for simulating the performance of several CPSD-SE commercial prototypes.

Table 6. Design specifications of the 25 kWe CPSD-SE system and 50MWe Jodhpur power plant

Specifications	Unit	Jodhpur power plant	Mohamed E. Zayed
Operating conditions			

Ambient Temperature	ºC	25	30
Solar radiation	W/m^2	1000	900
Stirling engine			
Stirling engine power	kWe	25	25
Working fluid	-	H_2	H_e
Receiver gas temperature	ºC	810	650-900
Engine speed	rpm	1800	1800
No. of cylinders	-	4	4
Bore and stroke	mm	44 × 57	55 × 40
Dish concentrator			
Rim angle	degree	39^0	45^0
Intercept factor	-	0.92	0.90
Mirror reflectivity	-	0.92	0.92
Un-shading factor	-	0.98	0.97
Cavity Receiver			
Cavity absorptivity	-	0.94	0.96
Receiver efficiency	%	93.89	82.336
Optical efficiency	%	77.88	66.13
Alternator			
Generator efficiency	%	92-94	92.5

Table 7. Data validation results of the CPSD-SE model

Description	The developed model	Actual published data at Jodhpur power plant	Error (%)	The developed model	Simulated published data by Mohamed E. Zayed	Error (%)
Total plant power, kW	50000	50000	0	25	25	0
Stirling efficiency, %	36.24	38.14	4.982	37.08	31.96	16.020
Aperture diameter, m	10.95	10.57	3.595	12.49	12.5	0.080
Projected area, m^2	94.23	91.01	3.538	122.5	122.75	0.204
Concentrator efficiency, %	82.95	82.94	0.012	80.32	80.316	0.00498
Focal length, m	7.485	7.45	0.470	7.511	7.54	0.385
Peak net efficiency, %	26.53	29.68	10.613	22.68	19.55	16.010
Rated output Power, kW	25	24.5	2.041	25	25	0

Performance Analysis

As aforementioned, to test the developed model and measure the performance of the system, the model has been implemented in a specific location, namely Mafraq, Jordan, and the meteorological data is obtained from the Solargis™ toolbox (Solargis, 2019). Figures 15-a, b show the annual solar radiation and wind speed data variation based on the hourly resolution in Mafraq. The wind speed varies between 2.3 m/s and 5.8 m/s, while solar radiation values range between 300 W/m^2 and 875 W/m^2.

Figure. 15 Solar and wind profile of Mafraq throughout one year.

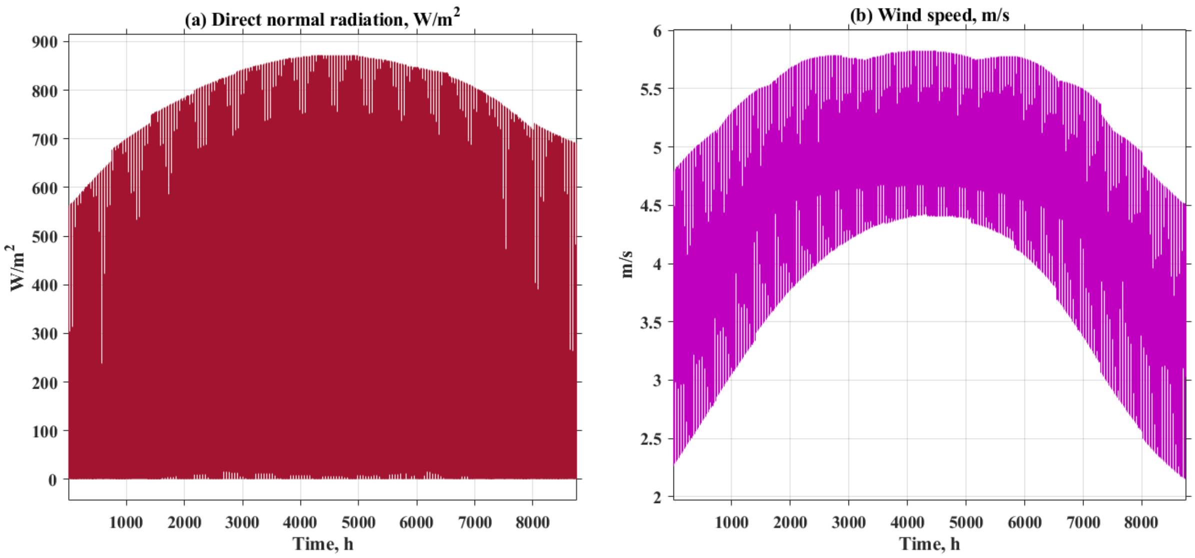

The MATLAB/Simulink® signal builder has been developed to represent the dynamic input battery model in order to specify the battery capacity as a function of the time throughout the year. The purpose of these generated Figures is to understand how 1-hour values spread over the year that assigned the battery charging and recharging cycle as depicted in Figure 16.

Figure 16. Charge/discharge rate signal of the batteries along (a) one day, (b) one month.

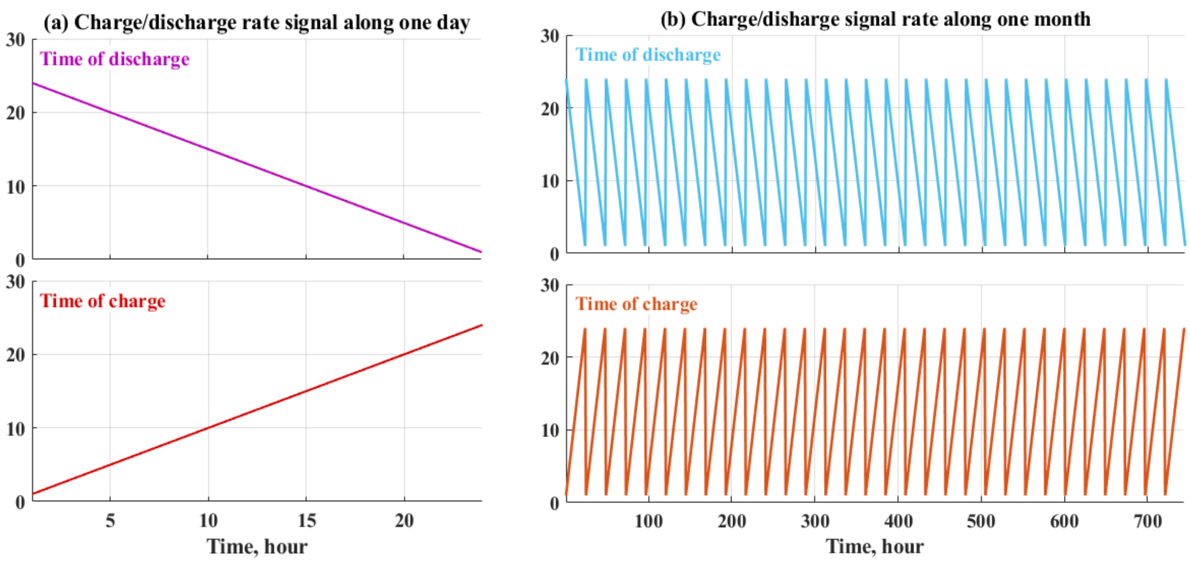

The control unit is in charge of distributing the load among the system units and the wind speed and solar radiation are the key variables that shape the load distribution. Figure 17 is the pseudo-algorithm that demonstrates the operation of the load distribution. If radiation from the sun exceeds the solar irradiance limitation (500 W/m^2), the signal prompts the CPSD-SE to operate without the assistance of wind turbines and/or the batteries bank. In case of the solar radiation is below the assigned solar limit and the average wind speed goes up the wind limitation (assumed to be 1.5 m/s), the HWT will enter into service instead of the CPSD-SE and/or the battery bank. In addition, the battery bank will serve the electrical demand when the charge rate is lower than 1, otherwise, the battery is charging along with HWT and CPSD-SE are operating.

Figure 17. Flow chart of the control

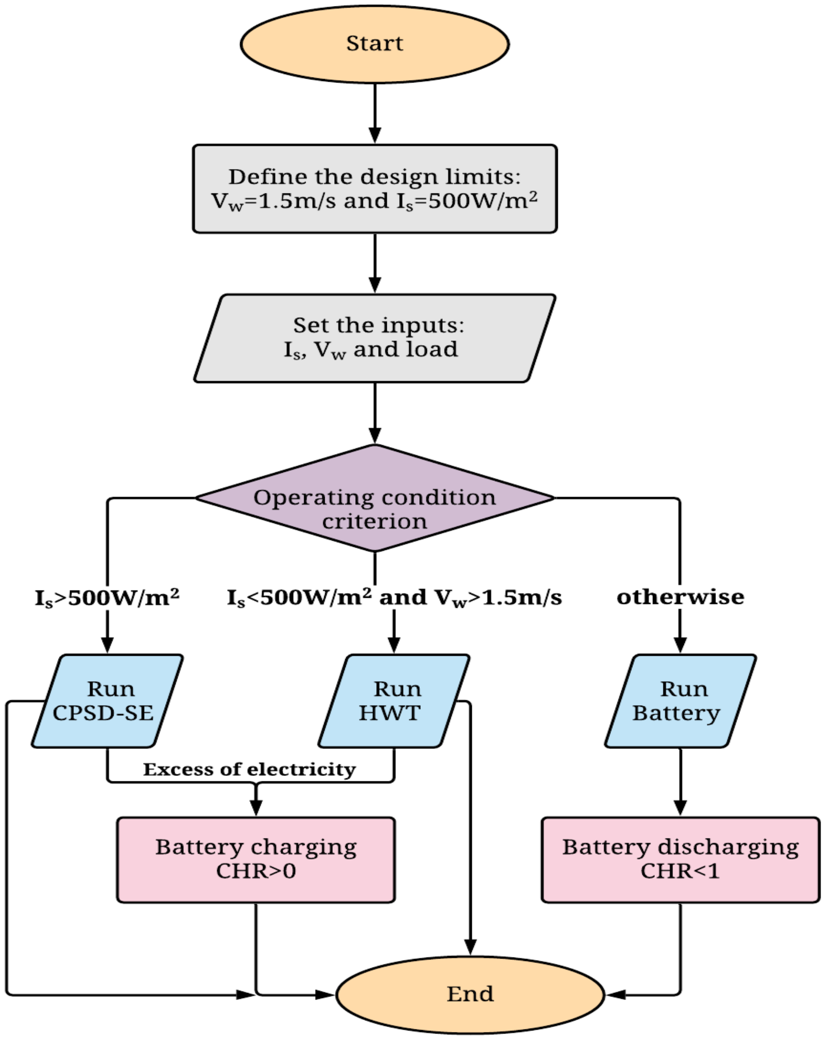

Figure 18 shows the hourly behaviour across one year (2018-2019) regarding the wind farm performance. The power developed was relatively high, depending on the wind speed variation. Therefore, the maximum total power generated by the wind farm marginally exceeds 890 kWe during the spring & summer times. The power coefficient (C_P) is in the range of 0.2 and 0.3, which is considered relatively high. The axial force is in the range of 19.3 and 32.4 kN/module and the net power from the module generator does not exceed 65 kWe.

Figure. 18 Data results related to the wind speed effect throughout one year (Mafraq, Jordan case study).

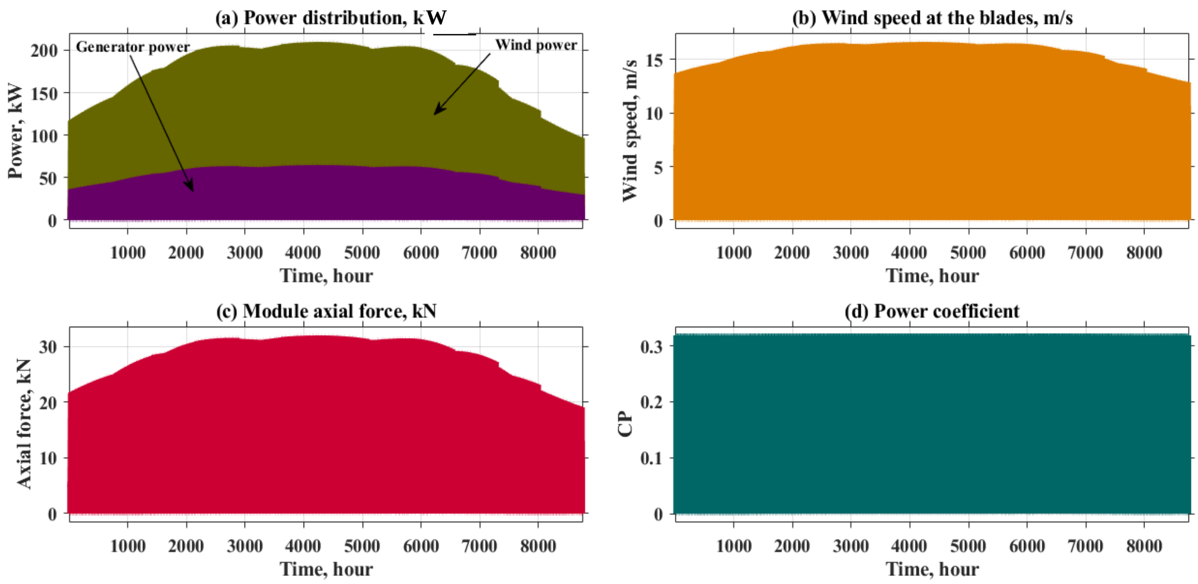

Figure 19 shows the results of the CPSD-SE unit. The power range is estimated to be about 1200 kWe. As an anticipated reflection of the solar radiation effect, Figure 19-b shows the top engine temperature throughout the year. The maximum allowable temperature is recorded during the summertime and it is between 590ºC and 605ºC. During the winter, the temperature drops, and it is between 460ºC and 515ºC. The CPSD-SE efficiency is in the range of 30% to 33% which is considered high when compared to the PV or solar gas turbine cycle. The engine compression ratio (CR_{SE}) and the pressure ratio (PR_{SE}) are attractive and in the range of 7.5-9.2 and 19-27.2, respectively, and this is because of the use of CO_2 instead of air that is commonly utilised (Sharaf Eldean et al., 2017). In addition, the fluctuations in the solar radiation have significantly affected the mean effective pressure, which is relatively high and equal to about 10.2, as indicated in Figure 19-f.

Figure 19. Data results related to the solar radiation effect throughout one year (Mafraq, Jordan case study).

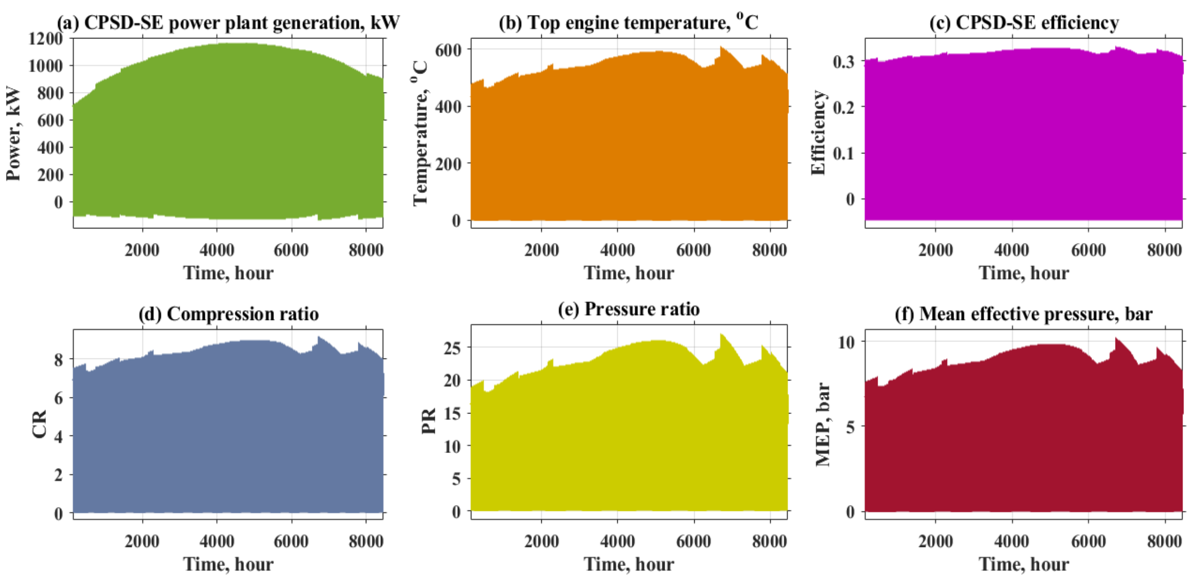

To examine the monthly performance, the predicted net average power production and the overall efficiency of the integrated power plant are shown in Figure 20. The results demonstrate that the high net power and overall efficiency values of the hybrid CPSD-SE/HWT system are obtained in the summertime between May and September.

Figure 20. Monthly net average output power and overall efficiency of the hybrid CPSD-SE/HWT system.

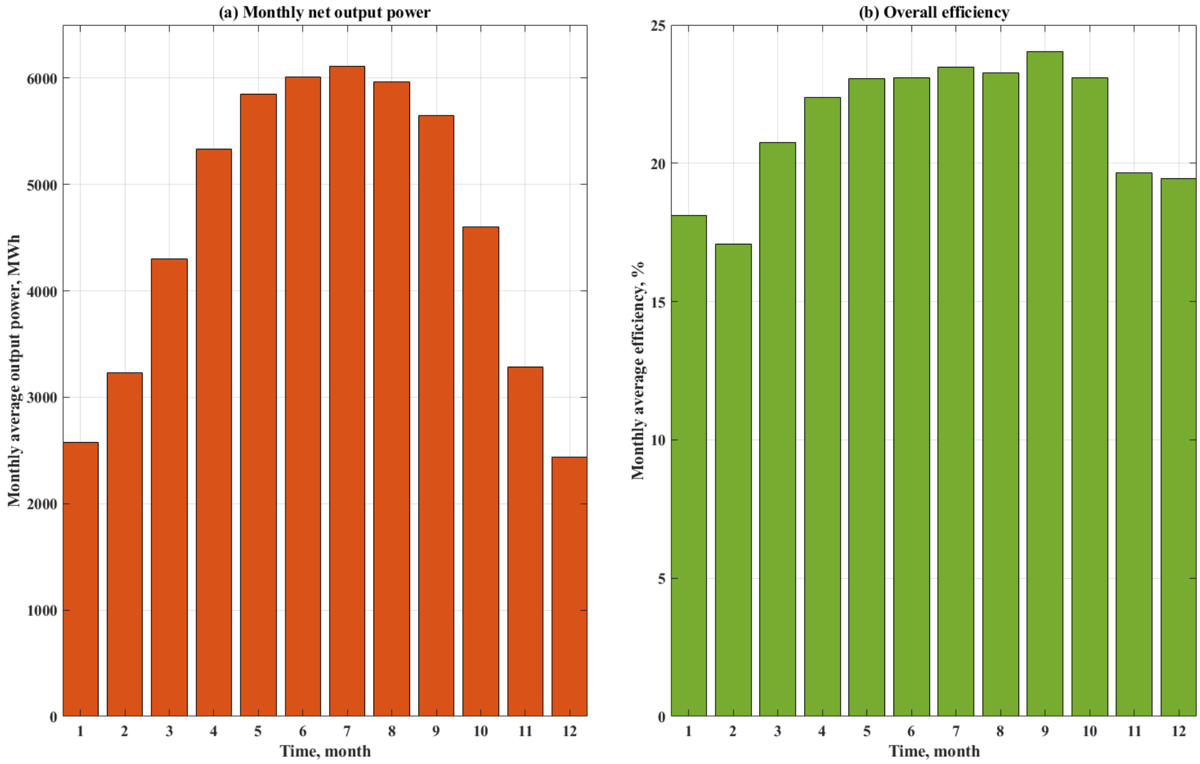

It can be seen that the monthly peak predicted the output power and the overall efficiency for the proposed power plant to be 6113.35 MWh and 24.03% in July and September, respectively. While the lowest power and efficiency values are recorded in the wintertime. The lowest output power is found to be about 2441.21 MWh in December, and the lowest overall efficiency in February, which is found to be 17.07%. Overall, it can be indicated that the average monthly net electricity production and average net monthly overall efficiency for the CPSD-SE/HWT plant are found to be about 4612.97 MWh and 21.45%, respectively.

In addition, Figure 21 shows a typical day in the summertime as an example. According to the fluctuations in the solar and wind energy generation, the Figure shows the variation in load generation across the whole day. From Figure 21, it is observed that the electricity demand surpasses the power generated from the proposed system that is produced during the day, particularly at night. Most of the day, the HWT generated a power range between 380 kWe and 900 kWe. The power generation in the middle of the day is dominated by the solar dish operation. The system starts at 5:20 am and provides 610kWe and ends with 590kWe at 16:30. In fact, throughout the period from 11:00 am to 01:00 pm, the peak power generated by the CPSD-SE is about 1200 kWe, as shown in Figure 21.

Furthermore, it is observed that batteries either produce or consume electricity throughout the day. The battery operates when there is no sun or wind, as shown in Figure 21. In this context, the batteries are discharging and delivering the electricity in the range of 100 to 375 kWe. Overall, it can be seen that the CPSD-SE has the potential to be an attractive system to generate power for residential communities; however, it needs a recovery unit such as a battery, and HWT. Table 8 shows some of the important calculated results under the Mafraq, Jordan operating conditions.

Figure 21. Power generation result related to 24-hour operation for a typical day in summertime in Mafraq, Jordan.

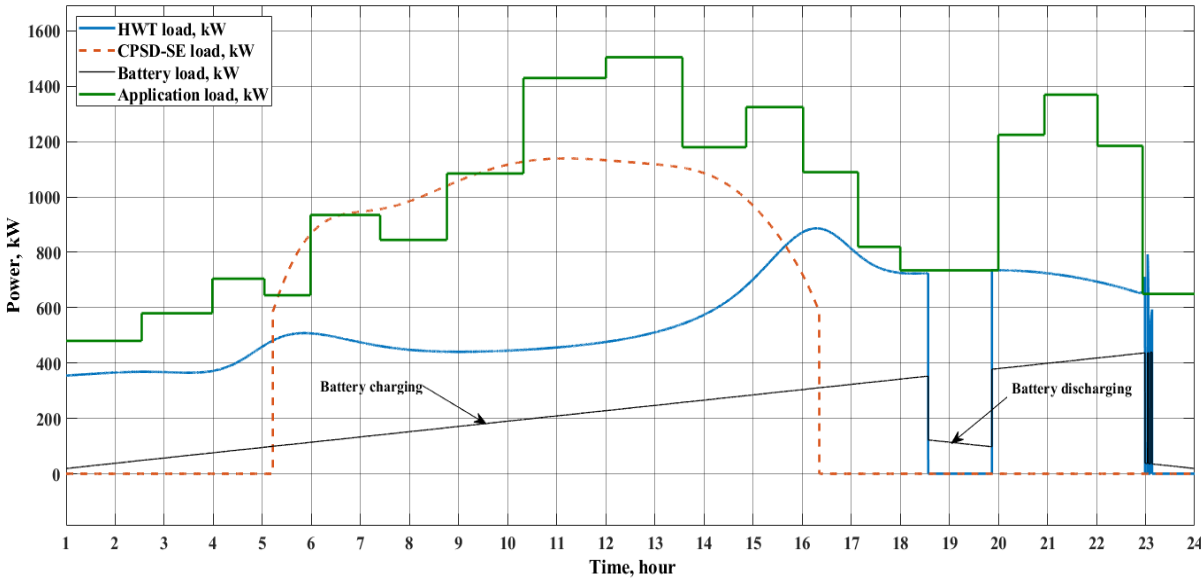

Table 8. Data results according to Mafraq, Jordan

Solar farm output		
Parameters	**Unit**	**Value**
Top engine temperature	ºC	506.50
Stirling efficiency	%	30.86
Total solar plant efficiency	%	22.75
Stirling engine power	kWe	16.86
Total plant power	kWe	1011.83
Electricity generation	MWh	11.13
Dish concentration ratio, A_d/A_r	-	1344.44
Total plant area	m^2	5702
Dish area	m^2	95
Stirling engine compression ratio	-	7.91
Stirling pressure ratio	-	20.73
Wind farm output		
Rotor swept area	m^2	1564.90
Torque	N.m	61216.83

Power coefficient	-	0.29
Wind power	kW	116.98
Mechanical power	kW	37.26
Net developed power per module	kWe	33.28
Total Farm Power	kWe	499.23
Electricity generation	MWh	11.98
Farm total area	km^2	0.54
Batteries bank output		
Total battery power	kWe	205.69
Electricity generation	MWh	4.94
Microgrid output		
Average overall efficiency	%	23.73
Net electricity production	MWh	17.34

The MATLAB/Simulink® was run to evaluate the hybrid CPSD-SE/HWT productivity throughout the year throughout the 8760 hours. Figure 22 shows the contribution of each sub-system, CPSD-SE, HWT, and batteries for power production. The predicted annual electricity generation of an application load 1500kWe capacity. Also, it demonstrates the dynamic behaviour of the generating electricity for system units during a full year to cover the load demand. The total annual electricity generated by the CPSD-SE, HWT, and battery bank varies from less than 700 kWe, 550 kWe, and 400 kWe to more than 1160 kWe, 900 kWe, and 420 kWe, respectively. As can be seen, despite the large energy output of the proposed system, it is not enough to cater for the current load demand, thus making the use of optimisation techniques an imperative action.

Figure 22. The power produced by the hybrid system over the year for Mafraq, Jordan.

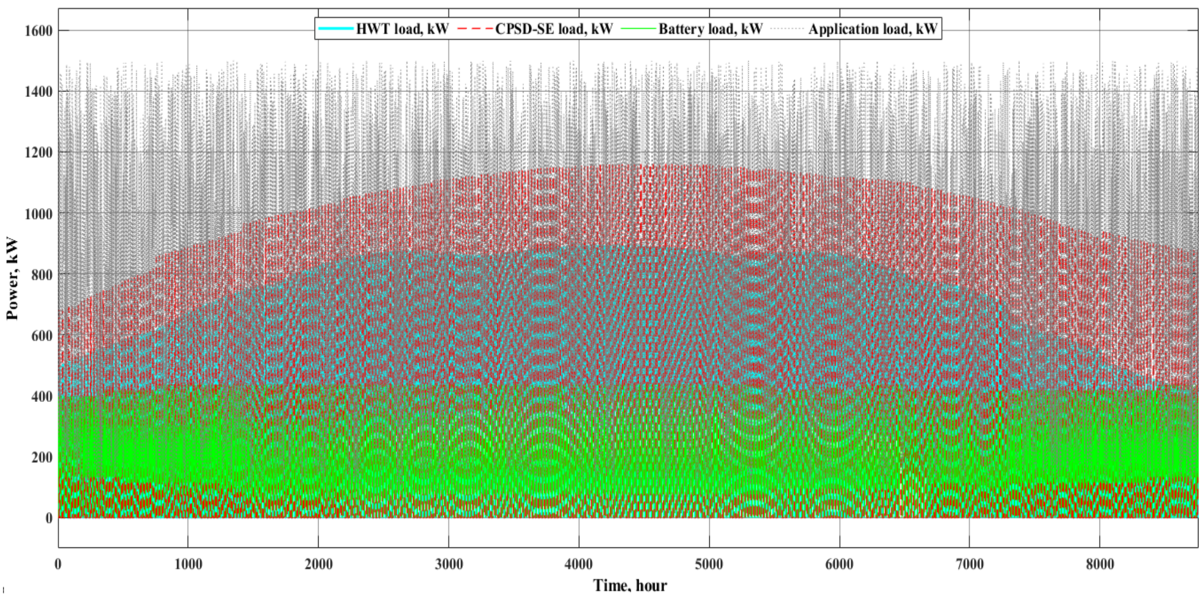

Economic Analysis

The economics of the entire microgrid system includes the total capital cost, total annual cost, total hourly cost, total LCOE, annual electricity savings and payback period. Table 9 presents the cost results for the investigated location (Mafraq). The cost-effectiveness of the hybrid system was examined based on the four economic indices of the whole system, including the total LCOE, $LCOE_{tot}$, *$/kWh*, total hourly cost, THC_{tot}, $/h, annual electricity savings, *AES*, *$* and payback period, *year*. These economic indicators are evaluated from Eqs. (1) to (4).

Overall, the total capital cost of the CPSE-SE/HWT system, including the total direct and indirect cost of the batteries bank, HWT and CPSD-SE is about 912772.84 $. The average LCOE of the hybrid system is found to be about 0.18 $/kWh and the average hourly costs are found to be 27.44 $/h. The estimated payback period for the integrated system is a year. It is evident that the developed system is feasible and competitive.

Table 9. Economic analysis results of the proposed microgrid systems configuration

Parameters	Unit	CPSD-SE	HWT	Batteries bank	Power plant
Total capital cost	$	18784.82	86527.74	950000	912772.84
Total annual cost	$/year	2759.89	10698.34	226875.99	240334.23
Total hourly cost	$/hour	0.32	1.22	25.90	27.44
Total LCOE	$/kWh	-	-	-	0.18
Annual electricity savings	$	-	-	-	828143.54
Payback period	year	-	-	-	1.03

Sensitivity Analysis

In general, the sensitivity analysis would be utilised to find out the optimal system behaviour related to various uncertain parameters. In this investigation, the four input variables are DNI, W/m^2, wind speed, *m/s,* rotor diameter, *m, and* dish diameter, *m,* that we have been taken to study their effects on the hybrid system results along the year. Table 10 shows the sensitivity variables that are used in the analysis. Each of the examined input variable impacts on the techno-economic performance results of the power plant, which are the $LCOE_{tot}$ and average overall annual efficiency as depicted in Table 10.

Table 10. Effect of the sensitivity variables on the proposed hybrid system

Sensitivity input variables	values	Sensitivity estimated variables
DNI	500-1000	$LCOE_{tot}$
Wind speed	1.5-6	Average overall annual efficiency
Rotor diameter	20-150	
Dish diameter	2-14	

Sensitivity to the Solar Radiation and Wind Speed

The average *DNI* was varied between 500 and 1000 W/m^2 and its effect on the LCOE$_{tot}$, *$/kWh* and total efficiency, *%*, may be observed (see Figures 23-a,b). The incident DNI has a moderate effect on the LCOE$_{tot}$ and average annual electricity generation, as shown in Figures 23-a and b. However, the solar radiation has a proportional effect on the average annual efficiency, the higher intensity of solar radiation, and the higher the overall efficiency, as depicted in Figures 23-b. In the case of increasing the direct solar radiation, the overall efficiency increases from 20.7% to 25.6%.

In the case of a variation in the wind speed, it has been observed that the wind speed played a key role in calculating the LCOE$_{tot}$. Accordingly, the wind speed was varied between 1.5 and 6 m/s. By considering Figure 23-a, it can be seen that the cost of electricity decreases with respect to the increase of solar radiation and wind speed, the LCOE$_{tot}$ varies between 0.188 $/kWh and 0.146 $/kWh. However, the wind speed also has a significant impact on the average net annual efficiency, the higher the wind speed, the higher is the overall efficiency, as illustrated in Figure 23-b.

Figure 23. Sensitivity of LCOE$_{tot}$ and net efficiency to the solar radiation and wind speed.

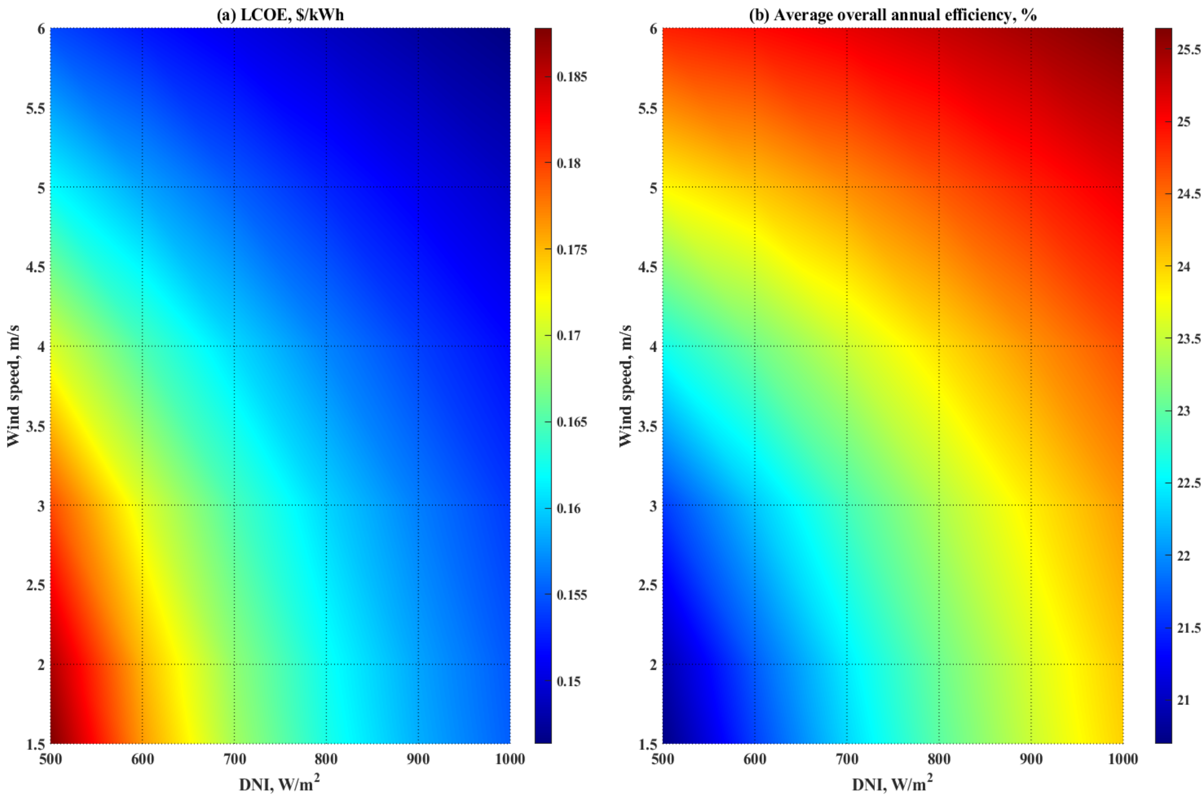

Sensitivity of LCOE$_{tot}$ and Overall Annual Efficiency to the *Rotor Diameter*

The effect of the rotor variation was analysed by MATLAB/Simulink® and in this study, the expected variation in the rotor diameter between 20 m to 150 m was considered. Thus, as the diameter increases then this has a significant change in the LCOE$_{tot}$ and the average overall annual efficiency. Figure 24 depicts the differing diameter variations impact on the economic indices and, as can be seen, the higher the diameter, the lower the LCOE. Hence, the increasing in the rotor diameter decreases the LCOE from 0.5668 $/kWh to 0.1206 $/kWh. As a result of comparing the simulation results with the increasing rotor diameter, it was found that the overall efficiency of power plant increases from 20.2% to 24.1%, as shown in Figures 24.

Figure 24. Sensitivity of $LCOE_{tot}$ and overall efficiency to the rotor diameter.

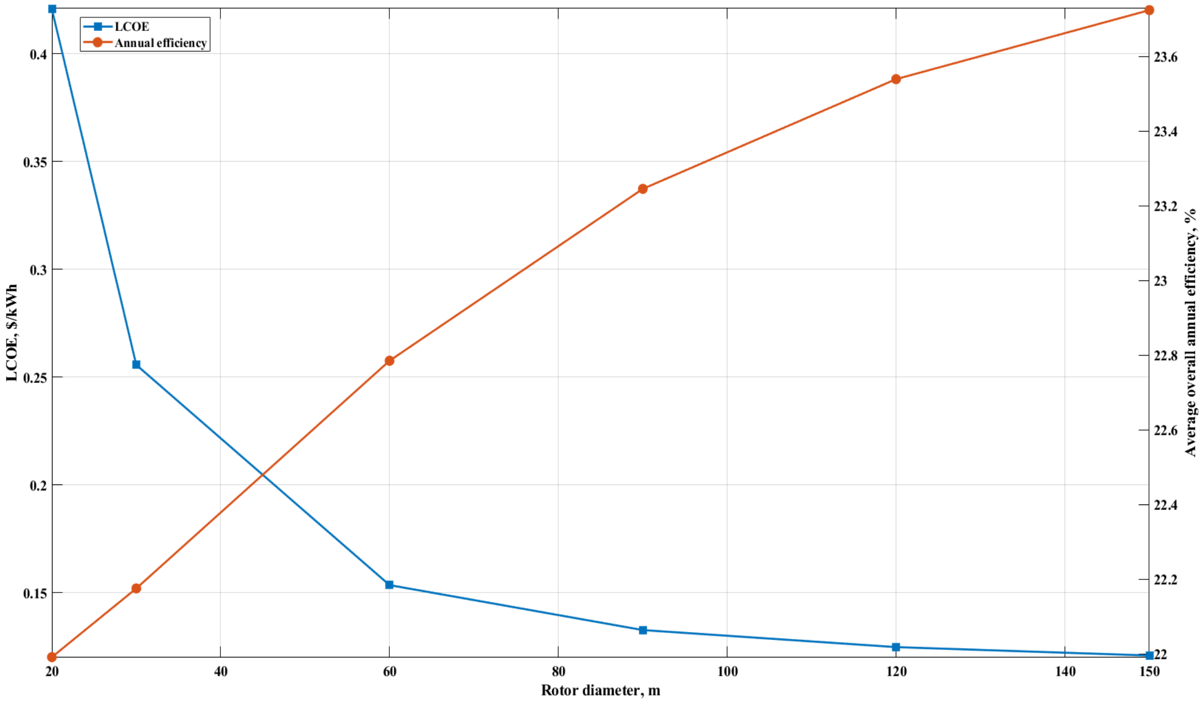

Sensitivity of $LCOE_{tot}$ and Overall Efficiency to the Top Cycle Temperature

The MATLAB/Simulink® is performed to investigate the effect of the high cycle temperature on the system performance and cost. The top cycle temperature is an important parameter when obtaining the most desirable outcome. The expected variation in the top cycle temperature is between 200 °C to 800 °C. As illustrated in Figure 25, it can be seen that a decrease in $LCOE_{tot}$ and an increase in the average overall annual efficiency with the top cycle temperature. Hence, the increasing of high cycle temperature decreases the $LCOE_{tot}$ from 0.1792 $/kWh to 0.1744 $/kWh. However, as the top cycle increases, it was found that the overall efficiency increases from 20.1% to 23.7%.

Figure 25. Sensitivity of $LCOE_{tot}$ and overall efficiency to the top cycle temperature.

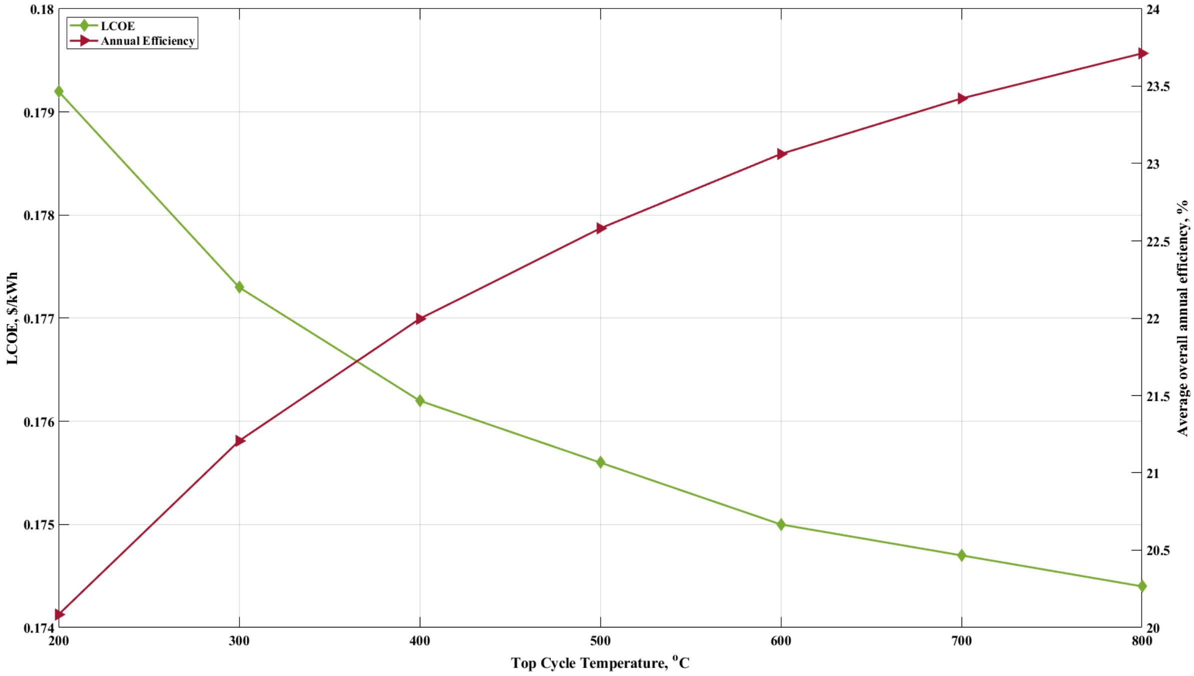

Multi-objective GA Optimisation Analysis

The developed GA model aims to determine the cost and efficiency range over a wide range of data related to the CPSD-SE/HWT power plant. Therefore, it would be very interesting to obtain optimised data that may help in the design and performance aspects. The optimisation model has been developed for two objective functions: $LCOE_{tot}$ (to be minimised) and plant efficiency (to be maximised).

The optimised data results for the entire CPSD-SE/HWT plant are obtained and analysed according to the input constraints listed in Table 3. To achieve the two objective functions, the performance constraints such as concentrator efficiency, η_c, %, receiver efficiency, η_r, %, and generator efficiency, η_{gen}, % are assumed to have the following values 97%, 80%, and 95%, respectively. These were anticipated to give optimal values related to the total efficiency and this is found to be 30.8% and in this case the $LCOE_{tot}$ is equal to about 0.248 $/kWh. The obtained results show that the number of dishes should be 54, the top cycle temperature is about 383 ^{o}C, the wind turbine power is 2.1 kWe, the number of wind turbines are 19 and the rotor diameter is 113 m. These mentioned design values are anticipated to achieve a higher total plant efficiency, η_{tot}, which is 30.8 %. For the operating conditions, to achieve the maximum of the total plant efficiency, it is assumed that the lower cycle temperature (sink) should be equal to 25 ^{o}C. However, solar radiation is assumed to be 875 W/m^2 , which is considered to be high.

It is quite clear that the GA would give a clear decision on the selection between the optimum $LCOE_{tot}$ and the optimum efficiency by specifying the optimum operating conditions and the design aspects needed (constraints).

Figure 26 indicates the Pareto front solution for the hybrid CPSD-SE/HWT with two objectives regarding the $LCOE_{tot}$ and η_{tot}. Each point on this Pareto front depicts a potentially optimum solution for the minimum $LCOE_{tot}$ and maximum η_{tot}. In this regard, the Pareto front assists the decision-maker in selecting a single ideal solution from a group of optimal solutions depending on the decision maker's preferences and criteria for establishing a microgrid CPSD-SE/HWT power plant with higher annual efficiency or a lower $LCOE_{tot}$. It is also indicated the impact of increasing the system efficiency on the Pareto front, dislocating the curves to higher values of efficiency, without significantly changing the values of the $LCOE_{tot}$.

As can be seen in Figure 26, all of the generated solutions occurred between (η_{tot} = 30.8%, $LCOE_{tot}$ = 0.248 \$/kWh) and (η_{tot} = 17.08%, $LCOE_{tot}$ = 0.207 \$/kWh). Hence, it can be indicated that the designer/decision maker can adopt various solutions for this case. From the shape of the curve it appears that solutions with higher efficiency should be preferred as the increase in the LCOE is not as sharp as the uplift of the energy efficiency.

Figure 26. Optimal Pareto fronts obtained for the two objective functions.

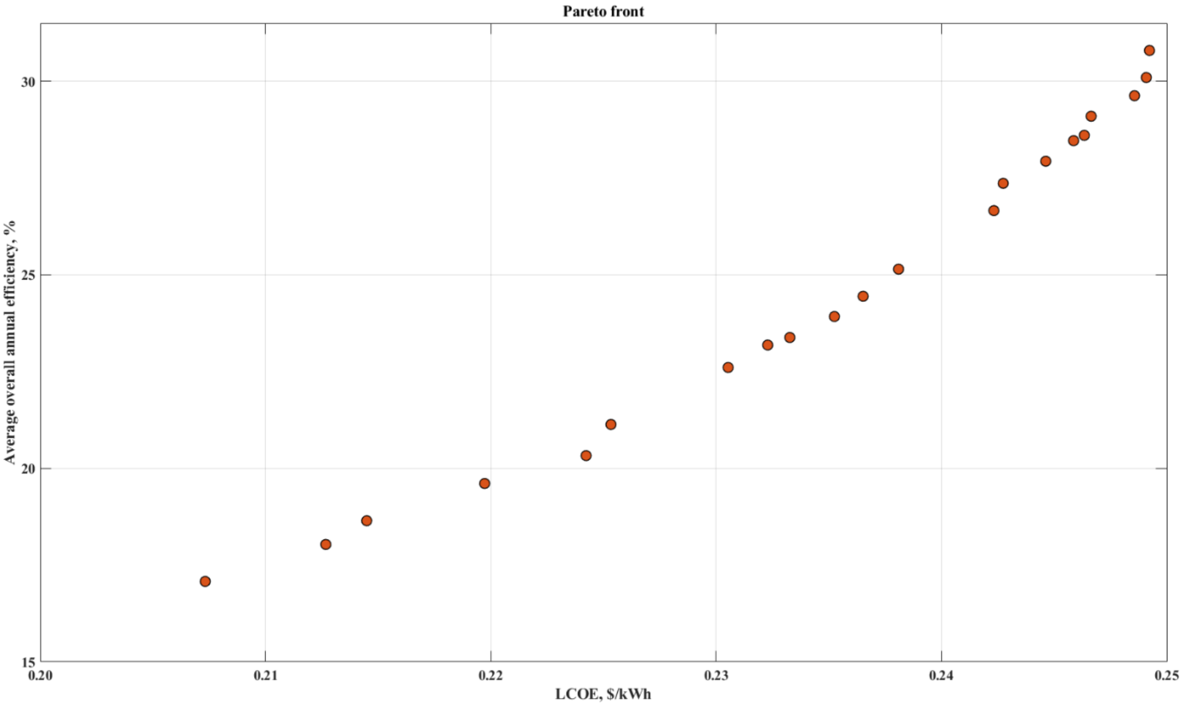

CONCLUSION

The aim of this study is to investigate advanced strategies for the integration, performance and optimisation of new hybrid CPSD-SE/HWT for stand-alone microgrid power generation. The system aims to supply power to arid and semi-arid regions and the system depends on the solar and wind energies. The annual simulation of a 1500 kWe hybrid system is performed dynamically for the city of Mafraq based on the operating conditions of the satellite-driven data from Solargis™. The integrated system is validated with the simulated and actual data published in the literature in order to ensure the reliability and accuracy of the developed model.

The results of the dynamic performance are presented. For the solar part, a CPSDE-SE has been considered and for the sun off periods, a HWT and a battery bank have been used. Regarding the CPSD-SE, CO_2 is used as the working fluid instead of air and a total number of 60 dishes are assumed to be implemented while the total number of HWTs is 7. For a typical summer day, during the daylight, the CPSD-SE is dominant and generates about 1500 kWe with a total high efficiency of about 26%. Most of the supplied power throughout the year is dominated by the CPSD-SE with a high cycle temperature that reaches up to 850^{o}C. On the other hand, the HWT generates a limited amount of power. However, it is considered to be extremely helpful to overcome the uncertainties in the solar radiation throughout the day.

A multi-objective GA method that is based on an evolutionary computation algorithm is applied to the CPSD-SE/HWT system for the electricity production to evaluate the optimal design parameters for the system. To fully utilise this, computer modelling techniques using the Multi-objective GA Solver in MATLAB/Simulink® have been employed. The objective functions, design parameters and constraints, and the overall optimisation are elaborated. The results show that the η_{tot} values are raged between 17.08% to 30.8%, where the $LCOE_{tot}$ values are about 0.207 to 0.248 $/kWh, thus, providing a set of optimal solutions for both objective functions to the designer. In general, this novel system could be substantially utilised as a distributed power generation system for a low to medium scale microgrid application.

ACKNOWLEDGEMENT

The authors would like to acknowledge Al al-Bayt University and the Oman Ministry of Higher Education for their valuable financial support.

REFERENCE

Agency, I. R. E. (2012). *Renewable Energy Technologies: Cost Analysis Series* (Vol. 1, Issue 2/5). https://doi.org/10.1016/B978-0-12-812959-3.00012-5

Ali, H. H., Al-rub, F. A. A., Shboul, B., & Moumani, H. al. (2020). *Evaluation of Near-net-zero-energy Building Strategies : A Case Study on Residential Buildings in Jordan*. *10*(6), 325–336. https://doi.org/10.32479/ijeep.10107

Ali, H. M. (2020). Recent advancements in PV cooling and efficiency enhancement integrating phase change materials based systems – A comprehensive review. *Solar Energy*, *197*(June 2018), 163–198. https://doi.org/10.1016/j.solener.2019.11.075

Badwawi, R. Al, Abusara, M., & Mallick, T. (2015). A Review of Hybrid Solar PV and Wind Energy System. *Smart Science*, *3*(3), 127–138. https://doi.org/10.1080/23080477.2015.11665647

Bakir, H., & Kulaksiz, A. A. (2020). Modelling and voltage control of the solar-wind hybrid micro-grid with optimized STATCOM using GA and BFA. *Engineering Science and Technology, an International Journal*, *23*(3), 576–584. https://doi.org/10.1016/j.jestch.2019.07.009

Belfkira, R., Zhang, L., & Barakat, G. (2011). Optimal sizing study of hybrid wind/PV/diesel power generation unit. *Solar Energy*, *85*(1), 100–110. https://doi.org/10.1016/j.solener.2010.10.018

Bernal-Agustín, J. L., Dufo-López, R., & Rivas-Ascaso, D. M. (2006). Design of isolated hybrid systems minimizing costs and pollutant emissions. *Renewable Energy*, *31*(14), 2227–2244. https://doi.org/10.1016/j.renene.2005.11.002

Cristóbal-Monreal, I. R., & Dufo-López, R. (2016). Optimisation of photovoltaic-diesel-battery stand-alone systems minimising system weight. *Energy Conversion and Management*, *119*, 279–288. https://doi.org/10.1016/j.enconman.2016.04.050

Diaf, S., Belhamel, M., Haddadi, M., & Louche, A. (2008). *Technical and economic assessment of hybrid photovoltaic / wind system with battery storage in Corsica island*. *36*, 743–754. https://doi.org/10.1016/j.enpol.2007.10.028

Dincer, I., Rosen, M. A., & Ahmadi, P. (2017). Optimization of energy systems. In *Optimization of Energy Systems*. https://doi.org/10.1002/9781118894484

Ding, Z., Hou, H., Yu, G., Hu, E., Duan, L., & Zhao, J. (2019). Performance analysis of a wind-solar hybrid power generation system. *Energy Conversion and Management*, *181*(September 2018), 223–234. https://doi.org/10.1016/j.enconman.2018.11.080

Dufo-López, R., Bernal-Agustín, J. L., Yusta-Loyo, J. M., Domínguez-Navarro, J. A., Ramírez-Rosado, I. J., Lujano, J., & Aso, I. (2011). Multi-objective optimization minimizing cost and life cycle emissions of stand-alone PV-wind-diesel systems with batteries storage. *Applied Energy*, *88*(11), 4033–4041. https://doi.org/10.1016/j.apenergy.2011.04.019

Erdinc, O., & Uzunoglu, M. (2012). Optimum design of hybrid renewable energy systems: Overview of different approaches. In *Renewable and Sustainable Energy Reviews* (Vol. 16, Issue 3, pp. 1412–1425). Elsevier Ltd. https://doi.org/10.1016/j.rser.2011.11.011

Global Solar Atlas. (2020, December 5).

Global Wind Atlas. (2020, December 4).

Guo, S., He, Y., Pei, H., & Wu, S. (2020). The multi-objective capacity optimization of wind-photovoltaic-thermal energy storage hybrid power system with electric heater. *Solar Energy*, *195*(August 2019), 138–149. https://doi.org/10.1016/j.solener.2019.11.063

Halabi, L. M., & Mekhilef, S. (2018). Flexible hybrid renewable energy system design for a typical remote village located in tropical climate. *Journal of Cleaner Production*, *177*, 908–924. https://doi.org/10.1016/j.jclepro.2017.12.248

Helioscsp. (2014). *225 MW from concentrated solar power in Jordan*.

Hirbodi, K., Enjavi-Arsanjani, M., & Yaghoubi, M. (2020). Techno-economic assessment and environmental impact of concentrating solar power plants in Iran. *Renewable and Sustainable Energy Reviews*, *120*. https://doi.org/10.1016/j.rser.2019.109642

Kabalci, E. (n.d.). *Hybrid renewable energy systems and microgrids*.

Kalantar, M., & Mousavi G., S. M. (2010). Dynamic behavior of a stand-alone hybrid power generation system of wind turbine, microturbine, solar array and battery storage. *Applied Energy*, *87*(10), 3051–3064. https://doi.org/10.1016/j.apenergy.2010.02.019

Keyif, E., Hornung, M., & Zhu, W. (2020). Optimal configurations and operations of concentrating solar power plants under new market trends. *Applied Energy*, *270*(May), 115080. https://doi.org/10.1016/j.apenergy.2020.115080

Khan, F. A., Pal, N., & Saeed, S. H. (2018). Review of solar photovoltaic and wind hybrid energy systems for sizing strategies optimization techniques and cost analysis methodologies. *Renewable and Sustainable Energy Reviews*, *92*(March), 937–947. https://doi.org/10.1016/j.rser.2018.04.107

Koutroulis, E., & Kolokotsa, D. (2010). Design optimization of desalination systems power-supplied by PV and W/G energy sources. *Desalination*, *258*(1–3), 171–181. https://doi.org/10.1016/j.desal.2010.03.018

Koutroulis, E., Kolokotsa, D., Potirakis, A., & Kalaitzakis, K. (2006). Methodology for optimal sizing of stand-alone photovoltaic/wind-generator systems using genetic algorithms. *Solar Energy*, *80*(9), 1072–1088. https://doi.org/10.1016/j.solener.2005.11.002

Kumar, R., Gupta, R. A., & Bansal, A. K. (2013). Economic analysis and power management of a stand-alone wind/photovoltaic hybrid energy system using biogeography based optimization algorithm. *Swarm and Evolutionary Computation*, *8*, 33–43. https://doi.org/10.1016/j.swevo.2012.08.002

Lagorse, J., Paire, D., & Miraoui, A. (2009). Hybrid stand-alone power supply using PEMFC, PV and battery Modelling and optimization. *2009 International Conference on Clean Electrical Power, ICCEP 2009*, 135–140. https://doi.org/10.1109/ICCEP.2009.5212069

Liu, H., Zhai, R., Fu, J., Wang, Y., & Yang, Y. (2019). Optimization study of thermal-storage PV-CSP integrated system based on GA-PSO algorithm. *Solar Energy*, *184*(December 2018), 391–409. https://doi.org/10.1016/j.solener.2019.04.017

Mohammadi, K., Khanmohammadi, S., Khorasanizadeh, H., & Powell, K. (2020). A comprehensive review of solar only and hybrid solar driven multigeneration systems: Classifications, benefits, design and prospective. *Applied Energy*, *268*(March). https://doi.org/10.1016/j.apenergy.2020.114940

Motevasel, M., Seifi, A. R., & Niknam, T. (2013). Multi-objective energy management of CHP (combined heat and power)-based micro-grid. *Energy*, *51*, 123–136. https://doi.org/10.1016/j.energy.2012.11.035

Nafey, A. S., Sharaf, M. A., & García-Rodríguez, L. (2010). Thermo-economic analysis of a combined solar organic Rankine cycle-reverse osmosis desalination process with different energy recovery configurations. *Desalination*, *261*(1–2). https://doi.org/10.1016/j.desal.2010.05.017

Olatomiwa, L., Mekhilef, S., & Ohunakin, O. S. (2016). Hybrid renewable power supply for rural health clinics (RHC) in six geo-political zones of Nigeria. *Sustainable Energy Technologies and Assessments*, *13*, 1–12. https://doi.org/10.1016/j.seta.2015.11.001

Ould Bilal, B., Sambou, V., Ndiaye, P. A., Kébé, C. M. F., & Ndongo, M. (2010). Optimal design of a hybrid solar-wind-battery system using the minimization of the annualized cost system and the minimization of the loss of power supply probability (LPSP). *Renewable Energy*, *35*(10), 2388–2390. https://doi.org/10.1016/j.renene.2010.03.004

Petrescu, S., Petre, C., Costea, M., Malancioiu, O., Boriaru, N., Dobrovicescu, A., Feidt, M., & Harman, C. (2010). A methodology of computation, design and optimization of solar Stirling power plant using hydrogen/oxygen fuel cells. *Energy*, *35*(2), 729–739. https://doi.org/10.1016/j.energy.2009.10.036

Rani, D., Jain, S. K., Srivastava, D. K., & Perumal, M. (2013). Genetic Algorithms and Their Applications to Water Resources Systems. In *Metaheuristics in Water, Geotechnical and Transport Engineering* (First Edit, Issue 1975, pp. 43–78). Elsevier Inc. https://doi.org/10.1016/B978-0-12-398296-4.00003-9

Rojas-Zerpa, J. C., & Yusta, J. M. (2015). Application of multicriteria decision methods for electric supply planning in rural and remote areas. In *Renewable and Sustainable Energy Reviews* (Vol. 52, pp. 557–571). Elsevier Ltd. https://doi.org/10.1016/j.rser.2015.07.139

Saffari, M., de Gracia, A., Fernández, C., Belusko, M., Boer, D., & Cabeza, L. F. (2018). Optimized demand side management (DSM) of peak electricity demand by coupling low temperature thermal energy storage (TES) and solar PV. *Applied Energy*, *211*, 604–616. https://doi.org/10.1016/j.apenergy.2017.11.063

SAM. (2021, February 18). *CSP Cost Data*.

Sharaf Eldean, M. A., Rafi, K. M., & Soliman, A. M. (2017). Performance analysis of different working gases for concentrated solar gas engines: Stirling & Brayton. *Energy Conversion and Management*, *150*(August), 651–668. https://doi.org/10.1016/j.enconman.2017.08.008

Shboul, B., AL-Arfi, I., Michailos, S., Ingham, D., AL-Zoubi, O. H., Ma, L., Hughes, K., & Pourkashanian, M. (2021a). Design and Techno-economic assessment of a new hybrid system of a solar dish Stirling engine instegrated with a horizontal axis wind turbine for microgrid power generation. *Energy Conversion and Management*, *245*. https://doi.org/10.1016/j.enconman.2021.114587

Shboul, B., AL-Arfi, I., Michailos, S., Ingham, D., Ma, L., Hughes, K. J., & Pourkashanian, M. (2021). A new ANN model for hourly solar radiation and wind speed prediction: A case study over the north & south of the Arabian Peninsula. *Sustainable Energy Technologies and Assessments*, *46*. https://doi.org/10.1016/j.seta.2021.101248

Singh, S., Singh, M., & Kaushik, S. C. (2016). A review on optimization techniques for sizing of solar-wind hybrid energy systems. In *International Journal of Green Energy* (Vol. 13, Issue 15, pp. 1564–1578). Taylor & Francis. https://doi.org/10.1080/15435075.2016.1207079

Solargis. (n.d.). *Solar resource maps of Jordan*. Retrieved July 3, 2020, from https://solargis.com/maps-and-gis-data/download/jordan

Starke, A. R., Cardemil, J. M., Escobar, R., & Colle, S. (2018). Multi-objective optimization of hybrid CSP+PV system using genetic algorithm. *Energy*, *147*, 490–503. https://doi.org/10.1016/j.energy.2017.12.116

Tafreshi, S. M. M., Zamani, H. A., Ezzati, S. M., Baghdadi, M., & Vahedi, H. (2010). Optimal unit sizing of distributed energy resources in microgrid using genetic algorithm. *Proceedings - 2010 18th Iranian Conference on Electrical Engineering, ICEE 2010*, 836–841. https://doi.org/10.1109/IRANIANCEE.2010.5506961

The Wind Power. (n.d.). Retrieved May 10, 2020, from https://www.thewindpower.net/windfarms_list_en.php

v. Siva Reddy, S. C. K. and S. K. T. (2012). Exergetic analysis and performance evaluation of parabolic dish Stirling engine solar power plant. *Archives of Thermodynamics*, *33*(4), 23–40. https://doi.org/10.1002/er

Wang, X. Q., Li, X. P., Li, Y. R., & Wu, C. M. (2015). Payback period estimation and parameter optimization of subcritical organic Rankine cycle system for waste heat recovery. *Energy*, *88*, 734–745. https://doi.org/10.1016/j.energy.2015.05.095

Xu, D., Kang, L., Chang, L., & Cao, B. (2005). *OPTIMAL SIZING OF STANDALONE HYBRID WIND / PV POWER SYSTEMS USING GENETIC ALGORITHMS*. *May*, 1722–1725.

Yang, H., Wei, Z., & Chengzhi, L. (2009). Optimal design and techno-economic analysis of a hybrid solar-wind power generation system. *Applied Energy*, *86*(2), 163–169. https://doi.org/10.1016/j.apenergy.2008.03.008

Yang, H., Zhou, W., Lu, L., & Fang, Z. (2008). Optimal sizing method for stand-alone hybrid solar-wind system with LPSP technology by using genetic algorithm. *Solar Energy*, *82*(4), 354–367. https://doi.org/10.1016/j.solener.2007.08.005

Yang, Y., Guo, S., Liu, D., Li, R., & Chu, Y. (2018). Operation optimization strategy for wind-concentrated solar power hybrid power generation system. *Energy Conversion and Management*, *160*(January), 243–250. https://doi.org/10.1016/j.enconman.2018.01.040

Yunus A. Çengel, M. A. B. (2015). *Thermodynamic an Engineering Approach* (8th ed.). McGraw-Hill Education.

Zayed, M. E., Zhao, J., Li, W., Elsheikh, A. H., Zhao, Z., Khalil, A., & Li, H. (2020). Performance prediction and techno-economic analysis of solar dish/stirling system for electricity generation. *Applied Thermal Engineering*, *164*(April 2019), 114427. https://doi.org/10.1016/j.applthermaleng.2019.114427

KEY TERMS AND DEFINITIONS

Concentration ratio: A ratio of the dish area to the receiver area.

Genetic Algorithm: A heuristic optimisation technique, which is biologically inspired using to find a set of optimal solutions.

Levelised Cost of Electricity: An economic parameter representing a cost per unit of electricity generated.

Microgrid: An autonomous and local energy network integrated with a central control system to generate power in multiple scales.

Power Coefficient: A parameter indicates the efficiency of wind turbine to convert the kinematic energy in the wind into electrical energy.

Rim Angle: A ratio of the focal length to the concentrator diameter.

Solar Dish: A solar thermal device producing high temperature to generate electricity.

APPENDIX 1 BATTERY BANK MATHEMATICAL MODEL (Shboul et al., 2021a)

Parameter	Equation
Single battery Amber hour, AH	$AH_b \times I_b \times t_d$
Single Battery storage, Wh	$E_b = AH_b \times V_b$
Single Battery power, W	$P_b = \frac{E_b \times DOD \times \eta_b}{OH \times NOC}$
Total battery bank power, W	$P_{b,tot} = P_b \times NOB$
Load current, A	$I_l = \frac{P_{b,tot}}{V_l}$

APPENDIX 2 HWT MATHEMATICAL MODEL (Shboul et al., 2021a)

Parameter	Equation
Air temp based on site elevation, ºC	$T_{air} = 15.5 - \frac{19.83 \times H_s}{3048}$
The air density, kg/m^3	$\rho = \frac{P_{air} \times 100}{0.287 \times (T_{air} + 273.15)}$
Air density at sea level, kg/m^3	$\rho_{air,s} = \rho \times e^{\left(\frac{-1 \times 0.297 \times H_s}{3048}\right)}$

Rotor swept area, m^2	$A_r = \pi \times \left(\frac{D_r}{2}\right)^2$
Air mass flow rate, kg/s	$M_{air} = \rho_{air,s} \times A_r \times V_{wr}$
Wind speed at the blades, m/s	$V_u = \frac{V_{wr}}{V_o/V}$
Power coefficient	$C_p = 4 \times \frac{V_{wr}{}^2}{V_u{}^2} \times \left(1 - \frac{V_{wr}}{V_u}\right)$
Required wind power, kW	$P_w = \frac{\left(\frac{1}{2} \times \rho_{air,s} \times A_r \times \left(Vw_r{}^3\right)\right)}{1000}$
Power delivered by the turbine, kW	$P_{mech} = P_w \times C_p$
Axial force on the turbine wheel, kN	$F_x = \frac{4}{9000} \times \rho_{air,s} \times A_r \times \left(V_{wr}{}^2\right)$
Rotor speed, rpm	$RPM_r = \frac{60 \times V_u}{\pi \times D_r}$
Rotor speed, *rev/s*	$\omega = \frac{(2 \times \pi \times RPM_r)}{60}$
Rotor torque, N.m	$T_{or} = \frac{(1000 \times P_{mech})}{\omega}$
Power outlet from generator, kW	$P_g = \frac{P_{mech}}{\eta_g}$
Output current, A	$I_g = \frac{1000 \times P_g}{\sqrt{3} \times V \times FP}$
Net power developed, kW	$P_{net} = P_{mech} - \left(RL \times P_g\right)$
Generator torque, N.m	$T_g = \frac{1000 \times P_{net}}{w}$
Total Farm power, kW	$P_{farm} = P_{net} \times N_{wt}$
Optimum spacing in a row, m	$X_s = 12 \times D_r$
Optimum spacing in cross-wind direction, m	$Y_s = 3 \times D_r$
total land area, km^2	$A_{t,tot} = 2 \times X_s \times Y_s \times N_{wt}$

APPENDIX 3 CPSD-SE MATHEMATICAL MODEL (Shboul et al., 2021a); (Sharaf Eldean et al., 2017)

Parameter	**Equation**
Piston volume, cm^3:	$V_p = Stroke \times \frac{\pi}{4} \times D_p{}^2$
Dish area, m^2	$A_{dish} = \frac{\pi}{4} \times D_c{}^2$
Stirling engine efficiency	$\eta_{SE} = 0.5 \times \left[1 - \left(\frac{T_l + 273}{T_h + 273}\right)\right]$
Total efficiency of the module	$\eta_o = \eta_{SE} \times \eta_{gen} \times \eta_c \times \eta_r$

Stirling engine compression ratio	$CR_{SE} = e^{\left(\frac{1 \times C_v}{R \times \left(\frac{\left(\frac{1-\frac{1}{\left(\frac{T_h+273}{T_l+273}\right)}}{\eta_{SE}}\right)-1}{1-\left(\frac{1}{\left(\frac{T_h+273}{T_l+273}\right)}\right)}\right)}\right)}$
Stirling high pressure, kPa	$P_h = 100 \times P_{atm} \times CR_{SE} \times \left(\frac{T_h + 273}{T_1 + 273}\right)$
Stirling pressure ratio	$R_{PSE} = \frac{P_h}{P_{atm} \times 100}$
Maximum specific volumes, m^3/kg	$v_{max} = \frac{R \times (T_1 + 273)}{100 \times P_{atm}}$
Minimum specific volumes, m^3/kg	$v_{min} = \frac{v_{max}}{CR_{SE}}$
Mean pressure, kPa	$P_m = \frac{P_{atm} \times (CR_{SE} + 1) \times (\left[\frac{T_h + 273}{T_l + 273}\right] + 1)}{4}$
Stirling engine power, kW	$P_{SE} = \frac{\eta_o \times I_s \times A_{dish}}{1000}$
Total plant power of CPSD-SE, kW	$P_{CPSD-SE} = N_{dishes} \times P_{SE}$
Top cycle temperature, ºC	$T_h = \frac{60 \times 10^9 P_{SE} \times (T_h + T_l)}{V_p \times NOC_{SE} \times P_{mean} \times \vec{V}_{SE} \times \pi \times (T_h - T_l)}$
Rim angle ratio, f/D_c	$RAR = 1.003 \times e^{-\left(\frac{\psi_r - 11.28}{13.86}\right)^2} + 2.186 \times e^{-\left(\frac{\psi_r + 100.2}{127.6}\right)^2}$
Focal length, m	$f = \frac{D_c}{4 \times tan\left(\frac{\psi_r}{2}\right)}$
Dish height, m	$H_{dish} = \frac{D_c{}^2}{16 \times f}$
Receiver area m^2	$A_r = \frac{\pi}{4} \times D_r{}^2$
Concentration ratio	$CR_{dish} = \frac{A_{dish}}{A_r}$
Total surface area, m^2	$A_{dish,tot} = A_{dish} \times N_{dishes}$

APPENDIX 4 COST ANALYSIS *(Shboul et al., 2021a)*

Economic parameters

Interest rate, %	$i = 5$
Battery lifetime, year	$LT_b = 5$
Amortization factor, 1/y	$A_f = \dfrac{i \times (1+i)^{LT_b}}{(1+i)^{LT_b} - 1}$
Plant lifetime, year	$LT_p = 25$
Fixed charge rate	$FCR = 0.098$
Batteries Bank	
Battery cost, $	$C_b = 100$
Variable operating cost of the batteries, $/kWh	$VOC_b = 0.07$ (Charging Electricity Price)
Direct capital cost of the batteries bank, $	$CC_b = 5 \times C_b \times N_b$, where N_b is No. of batteries.
Annual capital cost of the batteries bank, $/yr	$ACC_b = CC_b \times A_f$
Fixed operating cost of the batteries bank, $/y	$FOC_b = 0.05 \times CC_b$
Annual total cost of the batteries bank, $/yr	$ATC_b = ACC_b + FOC_b$
Hourly total cost of the batteries bank, $/hr	$HTC_b = \dfrac{ATC_b}{365 \times 24}$
Horizontal Axis Wind Turbine (HWT)	
Normalised capital cost, $/kWe	$POC = 1628$
Variable operating cost of the turbines, $/kWh	$VOC_t = 0$
Direct capital cost of the turbines, $	$CC_t = POC \times P_m$
Indirect capital costs of the turbines, $	$ICC_t = WTC + CTC + OCC$ *or* $ICC_t = 0.86 \times CC_t$
where, the wind turbine cost share: $WTC = 0.65 \times CC_t$, construction cost share (Civil works): $CTC = 0.16 \times CC_t$, and other capital cost share: $OCC = 0.05 \times CC_t$	
Total capital cost of the turbines, $	$TCC_t = CC_t + ICC_t$
Annual capital cost of the turbines, $/yr	$ACC_t = TCC_t \times A_f$
Fixed operating cost of the turbines, $/yr	$FOC_t = FCR \times CC_t$
Annual total cost of the turbines, $/yr	$ATC_t = ACC_t + FOC_t$
Hourly total cost of the turbines, $/hr	$HTC_t = \dfrac{ATC_t}{24 \times 365}$
Solar Dish Stirling Engine (CPSD-SE)	
SE cost, $/kWe	$CSE = 370 \text{ to } 400\$/kW$
Receiver cost, $/kWe	$CCR = 185\$/kW$
Dish concentrator cost, $/m^2	$CDC = 300\$/m^2$
Site cost is 2.2$/m^2	$SIC = 2.2\$/m^2$
Variable operating cost of the CPSD-SE, $/kWh	$VOC_{dish} = 0.06$
Direct capital cost of the CPSD-SE, $	$CC_{dish} = (COP \times P_{SE}) + ([CDC + SIC] \times A_c)$ Where $COP = CSE + CCR$
Indirect capital costs of the CPSD-SE, $	$ICC_{dish} = CPEC + CGC + OCC$

Where, the construction, procurement, and engineering cost share are calculated (H. M. Ali, 2020), (Agency, 2012): $CPEC = 0.16 \times CC_{dish}$, contingency cost share: $CGC = 0.10 \times CC_{dish}$, other capital cost share: $OCC = 0.03 \times CC_{dish}$	
Total capital cost of the CPSD-SE, $	$TCC_{dish} = CC_{dish} + ICC_{dish}$
Annual capital cost of the CPSD-SE, $/yr	$ACC_{dish} = TCC_{dish} \times A_f$
Fixed operating cost of the CPSD-SE, $/yr	$FOC_{dish} = FCR \times CC_{dish}$
Annual total cost of the CPSD-SE, $/yr	$ATC_{dish} = ACC_{dish} + FOC_{dish}$
Hourly total cost of the CPSD-SE, $/hr	$HTC_{dish} = \frac{ATC_{dish}}{24 \times 365}$
Total Plant Cost	
Total capital cost, $	$TCC_{tot} = CC_b + TCC_t + TCC_{dish}$
Total annual cost, $/y	$ATC_{tot} = ATC_b + ATC_t + ATC_{dish}$
Total hourly costs, $/h	$THC_{tot} = \frac{ATC_{tot}}{8760}$
Total variable operating costs, $/kWh	$VOC_{tot} = VOC_b + VOC_t + VOC_{dish}$
Total Levelised cost of energy, $/kWh	$LCOE_{tot} = \frac{THC_{tot}}{Load\ factor \times P_{tot}} + VOC_{tot}$
Annual electricity savings, $	$Electricity\ cost = LCOE_{tot} \times Annual\ electricity\ generated$
Payback period, year	$Payback\ period = \frac{TCC_{tot}}{Electricity\ cost}$

APPENDIX 5 THE DEVELOPED GA MULTI-OBJECTIVE FUNCTIONS

GA function code

- The Power coefficient function:

$$C_p = \left(4 \times \left(\frac{{V_{wr}}^2}{\left(\frac{V_{wr}}{V_o/V}\right)^2}\right) \times \left(1 - \left(\frac{V_{wr}}{\frac{V_{wr}}{V_o/V}}\right)\right)\right)$$

- The mechanical power delivered by the turbine, kW:

$$P_m = \left(\left(\frac{0.5 \times \left(\left(\frac{P_{air} \times 100}{0.287 \times \left(\left(15.5 - \left(19.83 \times \frac{H_S}{3048}\right)\right) + 273.15\right)}\right) \times exp\left(-1 \times 0.297 \times \frac{10}{3048}\right)\right) \times \left(\left(\frac{\pi}{4}\right) \times \left({D_r}^2\right)\right) \times \left({V_{wr}}^2\right)}{1}\right) \times C_p \times 1\right)$$

- The Stirling engine power, kW:

$$P_{SE} = \frac{\left(\left(0.5 \times \left(1 - \left(\frac{T_l + 273}{T_h + 273}\right)\right)\right) \times \eta_{gen} \times \eta_r \times \eta_c\right) \times DNI \times A_c}{1000}$$

- Total levelised cost of energy is obtained as:

$$LCOE_{tot} = \left(\left(\frac{\left(\frac{(140.5 \times NOB) + (0.230 \times POC \times P_m) + \left[\left(108.3 \times \left(\frac{\left(\left(0.5 \times \left(1 - \left(\frac{T_l + 273}{T_h + 273} \right) \right) \right) \times \eta_{gen} \times \eta_r \times \eta_c \right) \times DNI \times A_c}{1000} \right) \right) + (57.3 \times A_c) \right]}{8760} \right)}{LF \times (P_{SE} + P_{mech})} \right) + 0.13 \right)$$

- Average overall annual efficiency is calculated as:

$$\eta_{tot} = \frac{(P_{mech} + P_{SE}) \times 1000}{(DNI \times A_c \times N_{dishes}) + \left(\frac{0.5 \times 1.25 \times (\frac{\pi}{4} \times {D_r}^2) \times {V_w}^3}{1000} \times N_{wt} \right)} \times 100$$

APPENDIX 6 RANDOM NUMBERS WITHIN A SPECIFIC RANGE FOR LOAD CALCULATION

```
%% Hours:
% n = 8760 during the year.
% n = The number of hours (n=24*number of days in each month)
% n = 744 in Jan, Mar, May, Jul, Aug, Oct, Dec.
% n = 720 in Apr, Jun, Sep, Nov.
% n = 672 in Feb.

h1 = 1;
h2 = n;
Hour = sort(((h2-h1).*rand(n,1) + h1),'ascend');
```

```
%% Power, kW:
p1 = 100;
p2 = 1500;
Power = (p2-p1).*rand(n,1) + p1;
```